UNIVERSIDADE DE LISBOA
FACULDADE DE CIÊNCIAS
DEPARTAMENTO DE FÍSICA

Dynamics of Venus' atmosphere: wind characterization with Doppler velocimetry

Ruben Henrique Machado Gonçalves

Mestrado em Física
Especialização: Astrofísica e Cosmologia

Dissertação orientada por:
Pedro Mota Machado

2016

Aknowledgements

I decided to include this section to express my gratitude to those who support me and made possible my master degree.

I should start with my parents, Maria Teresa Machado e Henrique Gonçalves. They always supported my decisions, even when they disagreed, even when they truly believed that some decisions were not in my best interest. The decision to pursuit my dream of being an astrophysicist was accepted by them with great enthusiasm and with the belief that I could achieve my goals, that I had the capability to do it. They did everything they could to help me achieve this goal. We all desire to make our parents proud of us, I am doing it by fulfilling my dreams, I couldn't feel more happy.

There was a phase in my life that the idea of becoming an astrophysicist was just an impossible dream. But there was someone that understood my love for astrophysics, that I was about to live my life without giving myself a chance to follow my dream, that I was about to squander the possibility to achieve true fulfillment and happiness. My girlfriend, Joana Ramos Pereira, was responsible for making me realize that it was not impossible, that this was really my dream, that I did had the capability, that there was still time, and that I could create my own opportunity and could actually achieve my dream. She new I could do it before I knew I could.

I also want to thank my brothers, Daniel Gonçalves and Sérgio Gonçalves, for being my brothers! For their contribution in my education, for sharing my values, for helping me to know myself in ways that I couldn't do it myself. They helped me questioning (and get answers) about the meaning of life, what are we doing here, who am I, who do I want to be, where do I want to go. They guided (and still guide) my path in self-awareness and making the most of life.

Last, but not least, I am grateful to my supervisor, my guide, my teacher, my academic godfather, my friend, Pedro Mota Machado. I could not imagine to have someone, at this early stage of my career, that was more helpful, more generous, more "door opener" and a better friend, then he is. He trusted

in my capability and competence, gave me an opportunity to start as full-time researcher (my dream), taught me how to be a scientist. I hope this "partnerships" endures for many, productive, years, and I am sure that this friendship will last for life.

Thank you all.

This research his supported by the European Commission Framework Program FP7 under Grant Agreement 606798 (Project EuroVenus). I thank the VIRTIS/Venus Express team, the European Space Agency, and the Project EuroVenus. I also aknowledge the support of Faculdade de Ciências da Universidade de Lisboa (FCUL), the Fundação da Faculdade de Ciências de Universidade de Lisboa (FFCUL), and the Instituto de Astrofísica e Ciências do Espaço (IA) (where I hope to continue my work as astrophysicist for many years).

Abstract

The most relevant aspect of the general circulation of the atmosphere of Venus is its retrograde super-rotation. A full characterization of the zonal winds is crucial to understand this movement and the mechanisms that maintain it.

This thesis analyzes data from coordinated wind amplitude and variability measurements at Venus cloud-tops based on the two complementary techniques of Ground-based Doppler velocimetry (Widemann et al., 2007, 2008; Machado et al., 2012, 2014), using the ESPaDOnS instrument (Echelle SpectroPolarimetric Device for the Observation of Stars) at CFHT (Canada France Hawaii Telescope), and cloud-tracked winds using ESA Venus Express/VIRTIS-M (Visible and Infrared Thermal Imaging Spectrometer) imaging at 0.38 μm (Drossart et al., 2007; Sánchez-Lavega et al., 2008; **?**; Machado et al., 2014).

We performed a new coordinated campaign in April 2014 combining both Venus Express observations and ground-based Doppler wind measurements on the dayside of Venus' cloud tops at CFHT at a phase angle $\Phi = (76 \pm 0.3)^{\circ}$. The analysis and results show (1) additional confirmation of the complementarity, on both spatial and temporal time scales, of the two techniques ; (2) evidence of a symmetrical, poleward meridional Hadley flow in both hemispheres of $\overline{v}_m = 22.5 \pm 15.5$ ms^{-1}; (3) spatial and temporal variability of the zonal flow with latitude and local time, with a significant increase of wind amplitude near morning terminator already reported in Feb. 2011 observations.

This work complements the independent observations of the european space mission Venus Express and is part of the effort made by the scientific community in the area of planetology to understand the dynamics of the atmosphere of Venus.

Keywords: Venus; Atmospheres, Observational Techniques, Zonal Winds, Spectroscopy, Super-rotation.

Resumo em Português

Vénus

Vénus é o planeta mais próximo da Terra. Embora à primeira vista sejam planetas muito semelhantes (dimensão, densidade, massa, composição química), as condiçãos à superficie em cada um são bastante distintas. Se por lado, temos à suferficie da Terra uma temperatura média de ∼15°C e pressão atmosférica de 1 bar, já em Vénus a temperatura média é de ∼460°C e a pressão atmosférica de ∼90 bar, ou seja, uma temperatura superior à da fusão do ferro e uma pressão semelhante à verificada a uma profundidade de 1 km nos oceanos terrestres. Esta diferenÃ§a nas condições superficiais de cada planeta devem-se às diferentes características de cada uma das atmosferas - composição química, massa e moléculas condensáveis. Embora ambos os planetas e respectivas atmosferas tenham tido as mesmas condições iniciais, tenham evoluído da mesma nuvem proto-estelar, tenham passado pelos mesmo fenónemos de bombardeamente e de evolução do sistema solar, actualmente apresentam atmosferas bastante distintas. Se a pressão à superfície venusiana se deve à massa da atmosfera (∼92 vezes a massa da atmosfera terrestre), já o efeito de estufa descontrolado, originado pela quantidade dominante de CO_2 presente na atmosfera (cerca de 96%, comparativamente com o 0,034% de CO_2 na atmosfera terrestre), é responsável pela elevada temperatura superficial, mesmo considerando o albedo de cerca de 0.75 (75% da energia solar é reflectida e apenas 25% da radiação solar é absorvida pela atmosfera, contrastando com o albedo terrestre de 0,3).

A elevada temperatura à superfície de Vénus (a mais elevada de todo o Sistema Solar) constitui um notável caso de estudo para o aquecimento global e as subsequentes alterações climáticas. O estudo de climatologia comparativa entre Vénus e Terra deve ser encarado como essencial para a compreensão da evolução de atmosferas planetárias.

Para além das diferentes condições superificiais, há outras características que tornam Vénus diferente da Terra. O eixo de rotação é de 177,3°, sendo quase perpendicular ao plano da eclíptica, o que representa uma rotação retógrada (único planeta do sistema solar). O período de rotação do corpo

sólido é de 243 dias (terrestres), o que, considerando a rotação retrógrada, origina que um dia solar em Vénus (período entre dois consecutivas passagem do sol pelo mesmo meridiano local) seja de 117 dias (terrestres). Apesar deste facto, não se verificam variações de temperatura significativas entre os lados diurno e nocturno, isto porque, considerando a órbita quase circular e a pouca inclinação do eixo de rotação relativamente ao plano eclíptico (3°considerando o movimento retrógrado), ambos os lados recebem a mesma quantidade de energia no periodo de um ano (não hé estações do ano como as existentes na Terra).

A atmosfera venusiana está num estado de super-rotação, ou seja, tem um período de rotação (4,4 dias terrestres) muito inferior ao do corpo sólido do planeta (243 dias terrestres). A caracterização completa deste fenómeno dinâmico é crucial para compreender os mecanismos que a criam e a mantêm. A atmosfera está envolta por uma densa camada de nuvens formadas por gotículas de ácido sulfúrico e de um composto ainda não identificado que absorve a radiação ultravioleta. As nuvens, assim contrastadas, são traçadores quase ideais do movimento atmosférico, o que possibilita, através do seguimento dos seus movimentos, calcular a velocidade dos ventos. A atmosfera de Vénus contém aerossóis altamente reflectores em suspensão, ao nível da camada de nuvens que recobrem por completo o planeta, impondo-lhe um elevado albedo. Essas partículas são transportadas pelo vento, carregando assim consigo a informação relativa à dinâmica atmosférica. A presença dos gases e aerossóis que interagem com a radiação solar permite, por sua vez, realizar medições da velocidade do vento com base no estudo das riscas espectrais de absorção e de emissão, caso das técnicas Doppler heteródino no infravermelho e velocimetria Doppler com base na radiação solar visível dispersa pela camada superior das nuvens, sendo este último o método utilizado neste trabalho de tese. O projecto desenvolvido e aqui apresentado, centra-se no esforço para caracterizar a dinâmica atmosférica de Vénus utilizando observações realizadas a partir do solo, complementando assim as medições obtidas pelas missões espaciais.

Observações

Os trabalhos desenvolvidos neste projecto de investigação basearam-se em observações efectuadas com o Canada-France-Hawaii-Telescope (CFHT) em Mauna Kea no Hawaii, em Abril de 2014. Para estas observações foi utilizado o instrumento de espectroscopia de alta resolução *Echelle Spectro Polarimetric Device* (ESPaDOnS). O instrumento ESPaDOnS tem uma resolução espectral de R $\sim$ 80000 e cobre a banda do visível, com comprimentos de onda entre 310 e 1050 nm, registados num echelograma com 40 ordens

espectrais. O seu campo (FOV) é de 1,6 segundos de arco, equivalente a 507-520 km sobre o disco planetário para observações com um ângulo de fase entre 75.7° e 77.1°.

A partir dos espectros de alta resolução obtidos (na banda do visível, com comprimentos de onda entre 310 e 1050 nm), foi aperfeiçoada a técnica de medição directa de ventos a partir dos desvios Doppler nas riscas espectrais da radiação difundida pelo topo da camada de nuvens (a cerca de 70 km de altitude onde a profundidade óptica atinge a unidade). A correlação cruzada entre as riscas espectrais na atmosfera da Terra (riscas telúricas) e as riscas solares da radiação solar difundida ao nível do topo da camada de nuvens em Vénus (cerca de 7000 riscas solares de Fraunhofer) e uma dupla Gaussiana, permite obter o desvio Doppler resultante do movimento dos aerossóis presentes na atmosfera de Vénus e responsáveis pela dispersão da radiação solar. Os desvios Doppler medidos têm uma precisão, associada a cada uma das mediações efectuadas, de 5-10 ms^{-1}.

O ângulo de fase das observações de 2014 foi entre 75.7° e 77.1°, as bandas de latitude sondadas vão desde os 70°N e os 60°S em faixas de 10° de latitude. A zona sondada cobriu as longitudes +50° +36° +24° +12° e 0° em relação ao meridiano sub-terrestre, ao longo do lado diurno do planeta Vénus. A escolha das datas de observação permitiu combinar a necessidade de maximizar o diâmetro angular de Vénus (resolução espacial sobre o disco planetário) e minimizar o ângulo de fase da observação.

As observações de 2011 permitiram explorar o modelo zonal, meridional e da circulação entre o ponto sub-solar e o ponto anti-solar, através de um ajuste efectuado entre as velocidades obtidas e estes modelos de circulação ao longo de bandas de latitude entre o equador e as latitudes médias. As observações obtidas a partir do solo foram comparadas com as observações obtidas pelo *Visible and Infrared Thermal Imaging Spectrometer* (VIRTIS), instrumento a bordo da sonda orbital *Venus Express* (VEx) da Agência Espacial Europeia (European Space Agency - ESA). As observações de seguimento dos padrões de nuvens, efectuadas pela VIRTIS-M (no ultravioleta a 380 nm) a partir do espaço, incidiram no hemisfério Sul diurno, entre os 15°S e os 80°S, coordenada com as observações de solo. Os ventos Doppler obtidos usando quer o modelo de vento zonal único, quer o modelo com duas componentes de vento (zonal e meridional) revelaram uma boa concordância com os ventos obtidos a partir do método de seguimento de nuvens (*cloud tracking*).

Resultados

Os campos de velocidade medidos, no campo de latitudes e longitudes abarcado pelas observações, apresentaram uma velocidade média de $\bar{v_z} =$

119.6 ± 16.5 ms^{-1} em 16 Abr, de $\bar{v_z}$ = 122.6 ± 31.3 ms^{-1} em 17 Abr, de $\bar{v_z}$ = 119.6 ± 26.0 ms^{-1} em 18 Abr e de $\bar{v_z}$ = 118.1 ± 19.5 ms^{-1} em 19 Abr.

O perfil de vento zonal obtido é consistente com medições anteriores realizadas por sondas espaciais (Galileu, Pioneer Vénus, Vénus Express) com base no seguimento de nuvens, mas introduz muita informação relevante sobre a variabilidade do vento em hora local e latitude (dado o carácter inovador das medições serem instantâneas e simultâneas ao longo de uma vasta região sondada).

Nesta tese é ainda apresentada a primeira detectção a partir do solo de vento meridional, que engloba medições em ambos os hemisférios (a primeira medição foi efectuda por (Machado et al., 2012), mas incluia apenas medições do hemisfério norte). Os valores obtidos são: 22.5 ± 15.5 ms^{-1}, para os dados de 16 a 19 de Abril.

De modo a obter a melhor descrição possíbel do campo de velocidades de vento medida, os resultados obtidos foram comparados com vários models de circulação de vento e da sua caracterização nível do topo das nuvens.

A técnica utilizada na análise dos dados, permitiu a caracterização do vento zonal a nível latitudinal, em termos do seu perfil em função da hora local e da sua variabilidade temporal. Foi também investigada a presença de ondas planetárias de larga-escala e do seu papel na manutenção da super-rotação zonal.

Perto dos 50° de latitude foi detectada a presença de jactos atmosféricos moderados em ambos os hemisférios, send o do hemisfério Sul, mais intenso em cerca de 10 m/s. Constatámos que a velocidade baixa de forma significativa para latitudes acima dos 50°. Este trabalho complementa de forma independente as observações da sonda espacial Vénus Express, da ESA.

Os resultados de melhor ajuste para as velocidades obtidas revelam magnitudes de vento consistentes com medições prévias pelo método de seguimento das nuvens, dados povenientes das missões Pioneer-Vénus/OCPP (*Orbiter Cloud Photopolarimeter*), Galileo/SSI (*Solid State Imager*), VEx/VMC (*Venus Monitoring Camera)*and VIRTIS (*Visible and Infrared Thermal Imaging Spectrometer*) e por velocimetria Doppler (Widemann et al., 2007, 2008; Machado et al., 2012).

Os estudos, aqui apresentados, complementam de forma independente as observações da missão espacial Vénus Express, em particular no que diz respeito ao estudo da super-rotação atmosférica, circulação meridional e à sua variabilidade.

Palavras-Chave: Vénus; atmosferas, velocimetria de Doppler, vento

zonal, vento meridional, super-rotação.

Motivation

The consequences of (not) studying Venus' atmosphere

Venus is the closest planet from Earth and should be the most Earth-like planet we know: they have almost the same size, mass and density, they were formed at the same time, with the same ingredients, at almost the same location in the solar system. Yet, Venus has ended up with an extreme climate. Just by comparing surface conditions, one can realize that each planet followed a distinctive path at some point of evolution. One of the most relevant difference between the two planets is the atmosphere. The dense Venus' atmosphere (about 90 times the mass of Earth's atmosphere, yielding a surface pressure higher then Earth's one by the same factor) is dominated by CO_2, which is responsible for a runaway greenhouse effect and consequently high surface temperatures (reaching about 460°C).

By its proximity and paradoxical similarities/differences, Venus poses as key subject in our understanding of planetary evolution. Failing to understand why two almost twin planets had such different destiny means we will neither fully understand the conditions in which life appeared on Earth, nor apprehend the long-term evolution of our own climate, nor distinguish if an exo-planet is more Earth-like or Venus-like. Thus, the major key aspects in studying Venus' atmosphere are the follow:

- The comparative study of Venus and Earth atmospheric physics and dynamics may help us to understand the enormous differences that led planetary evolution in both planets and also constrain the prevision of their long-term atmospheric transformations.

- The study of Venus' runaway greenhouse effect should improve our understanding of the present climate change process taking place on Earth.

- Understanding the climate of Venus should be a prime task for planetary science as well as for the exoplanet community. Comparative

climatology between Venus and Earth will also contribute to constraining the concept of Habitable Zone (HZ) and its application to Earth-like exo-planets.

Contents

Aknowledgements **v**

Abstract **vii**

Resumo em Português **ix**

Motivation **xv**

1 Introduction - Venus **1**
1.1 Venus: Earth's false twin 1
1.2 Venus amtosphere 5
1.2.1 Composition 5
1.2.2 Dynamics and structure 6
1.2.3 Cloud deck 13
1.2.4 Comparative climatology 15
1.3 Earth's false twin: summary 15
1.4 Venus exploration 18
1.4.1 History of spacecraft missions 18
1.4.2 Venus Express 22
1.4.3 Akatsuki 27

2 Methods: Doppler Velocimetry and Cloud Tracking **29**
2.1 Doppler velocimetry 29
2.1.1 Method Summary 30
2.1.2 Projected Radial Velocities 31
2.1.3 Fraunhofer absortion lines at Venus and Earth 31
2.1.4 Wind radial velocity 33
2.1.5 Young effect 34
2.1.6 Instrumental spectral drift 34
2.1.7 Error estimate 35
2.1.8 Pointing accuracy 37

2.1.9 Sensitivity tests . . . 38
2.1.10 Kinematical wind models . . . 41
2.1.11 Altitude of measurments . . . 43
2.2 Cloud Tracking . . . 44
2.2.1 Cloud tracking method . . . 45

3 Telescope and Instrument **47**
3.1 Telescope - CFHT . . . 47
3.2 Intrument - *ESPaDOnS* . . . 47
3.2.1 Instrument description . . . 47
3.2.2 Modes . . . 49
3.2.3 Wavelength calibration . . . 50

4 Observations **53**
4.1 CFHT/ESPaDOnS observations . . . 53
4.1.1 Geometry . . . 53
4.1.2 Data reduction . . . 55
4.2 VEx/VIRTIS-M observations . . . 58

5 Results **63**
5.1 CFHT/ESPaDOnS results . . . 63
5.1.1 Mean zonal circulation . . . 63
5.1.2 Meridional wind . . . 66
5.1.3 Zonal wind variability (spatial and temporal) . . . 68
5.2 VEx/VIRTIS-M results . . . 75
5.3 Intercomparison of results (CFHT/VEx) . . . 77
5.3.1 Long-term comparison . . . 77

6 Discussion and Conclusions **81**
6.1 Discussion . . . 81
6.2 Conclusions . . . 83

Chapter 1

Introduction - Venus

1.1 Venus: Earth's false twin

In a first approach Venus and Earth are similar planets. Having originated from the same "cloud" of gas and dust, Venus and Earth formed at roughly the same time, evolved from the same proto-solar nebula, have endured the same statistical debris bombardment in the early solar system (as icy planetesimals, cometary-like bodies or rocky asteroids), have similar densities, size, mass and bulk chemical composition (table 1.1). Despite solar system's formation arguments that sustain the similarity of initial atmospheric conditions for Venus and Earth they evolved in radically different ways (Grinspoon, 1997). One major difference resides in the rotational motion. Venus is the only planet with retrograde rotation in the solar system, with an obliquity of 177°. This means that its rotational axis is almost perpendicular to the ecliptic. The two hemispheres receive approximately the same amount of radiation over the year, thereby seasonal variations are negligible (Bougher et al., 1997).

Other differences can be seen at the surface conditions. The average temperature in Venus's surface is about 460°C (this is higher than the melting temperature of lead) and the pressure is about 90 times the atmospheric pressure in Earth's surface (the equivalent pressure found at a depth of 1 km in Earth's oceans), with a visual horizon that does not extend beyond 400 meters in a yellowish desolated world (possibly due to sulphur compounds, (Grinspoon and Bullock, 2007)). Thermodynamically speaking, the pressure and temperature at surface led the atmospheric properties to be closer to the liquid phase than the gaseous one. This is the case of its major compound, CO_2, which has its critical point at a temperature of 304°K and a pressure of 73 bars, so at the first scale height of Venus atmosphere (at about 16 km

	Earth	Venus
Radius (km)	6378	6051
Density (g/cm^3)	5.5	5.3
Distance to Sun (UA)	1	0.72
Sidereal Year (days)	365	226 (0.62year)
Rotacional Period (days)	1	243 (ret)
Obliquity (°)	23.5	177
Solar Constant	1380	2620
Albedo	0.3	0.75
Equilibrium Temperature (°C)	-15	15
Surface Temperature (°C)	15	460
Surface Pressure (atm)	1	92
Atmospheric Composition	78.1% N_2 20.9% O_2 0.034% CO_2	96% CO_2 3% N_2
Atmospheric Condensables	H_2O	H_2SO_4

Table 1.1: Earth and Venus physical and atmospheric characteristics. (left: Earth; right: Venus).

altitude), the carbon dioxide is a supercritical fluid (Kastings, 1988).

Venus is also the slowest moving planet, a fact which is made evident by looking at its poles. Whereas every other planet in the Solar System has experienced flattening at their poles due to the speed of their spin, Venus has experienced no such flattening. One Venusian day is about 243 Earth days. Considering its retrograde motion as well, Venus has a solar day of about 117 Earth days (Grinspoon, 1997), i.e., it takes about 117 Earth days for an observer (stationary) at Venus surface to see two consecutives Sun rises. So, any location at the Venus equator will be at day time for about 59 Earth days, and the same period for night time. Although this could indicate a high temperature gradient from the day side to the night side, the temperature is quite homogeneous at the entire surface. Due to the low inclination of the rotational axis relatively to the ecliptic (about 3° considering the retrograde rotation), and an almost circular orbit, the two hemispheres receive approximately the same amount of radiation over the year, thereby seasonal variations are negligible - there are no season as we have on Earth (Bougher et al., 1997).

Why is Venus so hot?

Although Venus is closer to the Sun, its albedo (0.9) is much bigger than Earth's albedo (0.3). Thus, from the total radiation that Venus receive from the Sun, about 90% is reflected. If we consider Venus as a black body and also take into account its albedo, the surface temperature value would be of about -90°C (this calculus would exclude any greenhouse atmospheric effects) - Venus would be cooler than Earth. So, the major contribution for the high surface temperature in Venus is its atmosphere. The dense atmosphere, high concentration of CO_2 and the consequent strong greenhouse effect causes the planet infrared radiation to be trapped and reabsorbed. It is yet unclear in the surface temperature has ever been low enough to allow condensation of water, even in possibly reduced solar illumination conditions in the early solar system (Chassefière et al., 2012). These facts make Venus the prime case study for comparison with Earth.

Plate tectonics

Venus doesn't have plaque tectonics like Earth. Since Venus has lost its water, it has become a more rigid, low viscosity body, and so, the plaque dynamics are more standstill - it is a single-plated planet (Bengtsson and Grinspoon, 2013). One significant difference is that the core of Venus shows evidence of being solid and comparatively much colder than the Earth's core (Lewis, 2004). There are major periodic volcanic events in Venus surface, but they happen at a planetary scale. In the Earth's case, the plate tectonics mechanism is closely linked to the carbon dioxide cycle, literally burying large amounts of it at subduction zones, stabilizing in this way the atmospheric CO_2 (Holland, 1978). Such a process would not occur in the single plate Venus' crust.

Magnetosphere

Planets which generate magnetic fields in their interiors, such as Earth, Mercury, Jupiter and Saturn, are surrounded by invisible magnetospheres. Their magnetic fields deflect the charged particles of the solar wind (electrons and protons) as they stream away from the Sun. This deflection creates a magnetosphere - a protective "bubble" around the planet - which ends in an elongated magnetotail on the lee side of the magnetosphere. Venus does not internally generate a magnetic field. As on Earth, solar ultraviolet radiation removes electrons from the atoms and molecules in the upper atmosphere, creating a region of electrically charged gas known as the ionosphere. Since Venus has no intrinsic magnetic field to act as a shield against incoming

charged particles, the solar wind sometimes interacts directly with the upper atmosphere. The evidence of a weak magnetic field around the planet, suggested the hypothesis of a magnetosphere generated, not by a dynamo effect, as on Earth, but rather by the interaction of solar wind with the charged particles of the ionosphere (Goody et al., 1975) - an induced magnetic field (figure 1.1). Venus' magnetosphere is weaker than Earth's and closer to the planet.

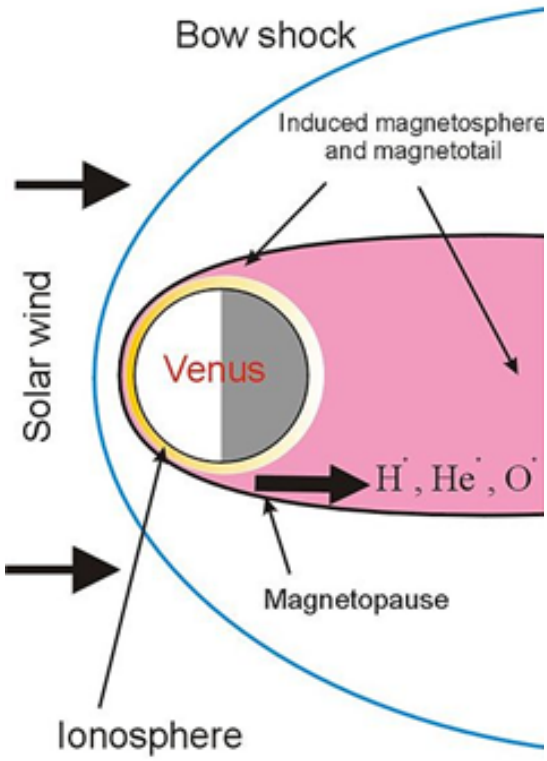

Figure 1.1: Bowshock of the interaction between the plasma particles of solar wind and the induced Venus' magnetosphere..

1.2 Venus amtosphere

1.2.1 Composition

After formation, Venus, Earth and Mars had presumably similar atmospheres, both in primordial composition and in relative abundances of its constituents. On Venus, most of the carbon dioxide is still present in the atmosphere (figure 1.2), contributing to a massive greenhouse effect, which makes it an extreme case study of the possible consequences of climate change on Earth, given the present day problems of anthropogenic excess emission of greenhouse gases.

If in the one hand Venus is a "CO_2 dominated" planet, on the other hand, its atmospheric balance is fine-tuned by the SO_2 concentration (among other minor components) at this evolutional stage of present atmospheric conditions (Bullock and Grinspoon, 2001). One of the minor components of extreme importance in the atmosphere/surface coupling (as already mentioned) is the Sulphur dioxide (SO_2). It is also worth noting the source of another minor component, the carbon monoxide (CO), in the upper atmosphere due to the photolysis of CO_2. These molecules tend to sink in the clouds toward the surface, over a timescale of weeks. It was also found evidence of the existence of H_2O in the upper atmosphere, but only at trace level (Beatty et al., 1999). Due to the loss of Venus' atmospheric CO_2 by photolysis in the upper atmosphere, H_2O also by photolysis and SO_2 in the reactive process of sulphuric acid formation, it is necessary to have some source for these molecules. Volcanism is the elected candidate for the replenishment process and for their temporal abundance variability as well. During the episodic large-scale volcanism, the atmosphere is injected with large amounts of these molecules.

The surface-atmosphere interactions were also a major factor for the different planetary evolution path followed by Earth and Venus. While on Earth there is a CO_2 absorption by the oceans, on Venusian there is an outgassing of volcanic sulphur into the atmosphere. Chemical reactions with the surface of Venus deposit SO_2 on the ground, so to keep the dynamic atmospheric balance it is necessary to have a source of replenishment (Bullock and Grinspoon, 2001). It is here that fits the extensive volcanism evident in the Venus' surface. A closer examination of the chemical reactions that affect the Venus' atmospheric gases, shows that these constituents are in equilibrium with the rocks on the planet's surface. This means that the chemical composition of the Venus atmosphere is determined by the properties of the surface, which does not happen in Earth. The reason for this different behavior lies in two factors: (1) on Earth there are destabilising processes such as photosynthesis,

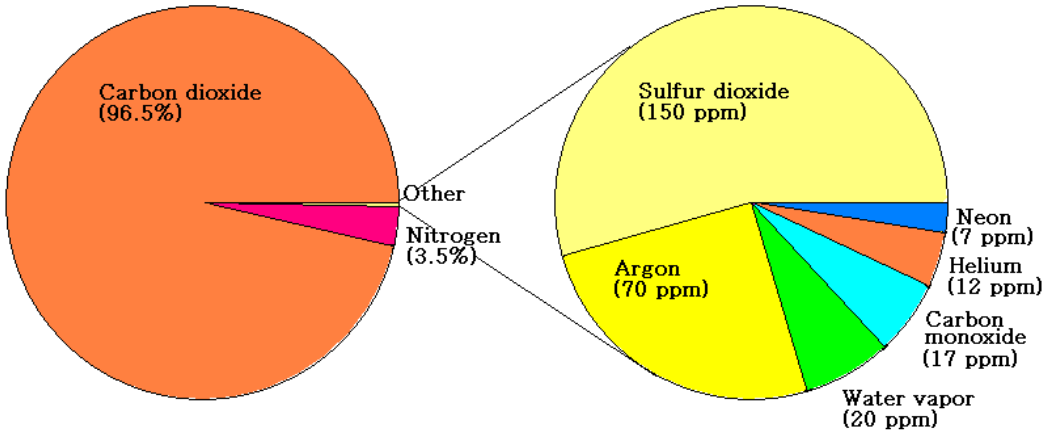

Figure 1.2: Venus atmosphere relative composition. Minor species relative abundances are given in the magnified portion of the graphic at the right side. (figure: NASA website).

perturbing CO_2 levels; (2) the very high Venus' surface temperatures that leads to fast chemical reactions between atmospheric gases and rocks, thus chemical equilibrium is reached quickly (Goody et al., 1975; Fegley et al., 1997).

1.2.2 Dynamics and structure

The atmosphere of Venus is extremely dense. The total mass of the atmosphere on Venus represents approximately 92 times the mass of Earth's atmosphere, despite the planets size similarity. Thus, the atmospheric pressure on the surface of Venus is about 92 bar. The atmosphere of Venus is in super rotation, a state in which its averaged angular momentum is much greater than that corresponding to co-rotation with the surface. The rotation of the solid planet (with a period of 243 terrestrial days - citepMueller2011) contrasts dramatically with the much faster clouds rotation, which circle the planet in only 4.4 days at 70 km altitude and about 6 days at 48 km. While on Earth the total surface coverage by clouds is only, on average, 40%, on Venus, it reaches 100%. The surface is hidden by a thick hazy cloud cover that results from the chemical interaction between sulphur dioxide and some water vapour that generates droplets of sulphuric acid. Venus atmospheric dynamics is essentially driven by thermal heating and by its low rotation rate. As a consequence from its low rotational velocity, the Venus' atmospheric dynamics major mechanisms are quite different from Earth. We define the components of the wind to be a zonal wind u (along the isolati-

tude lines), a meridional wind v (along the meridians), and a vertical wind w (upwards). There are three major atmospheric global circulation processes that characterize the Venus atmospheric dynamics:

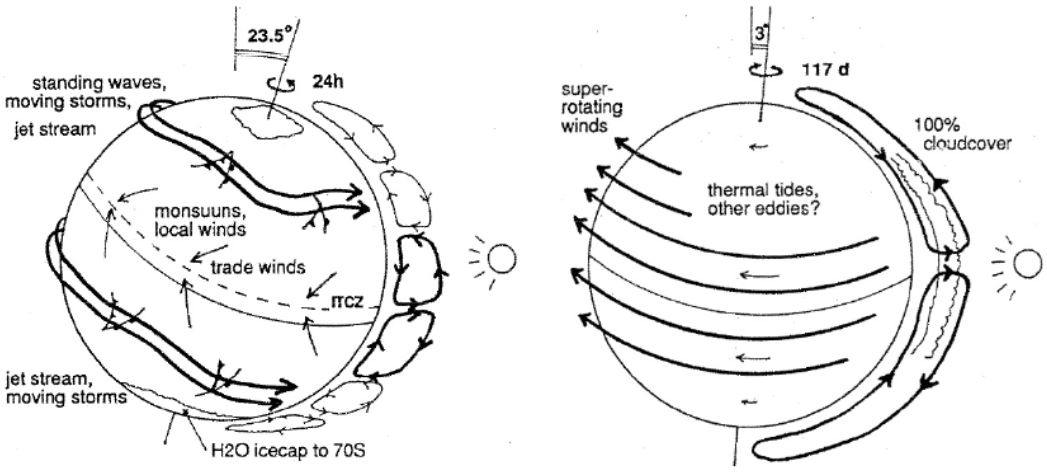

Figure 1.3: Large-scale motion of planetary atmospheres are dominated by various types of circulation patterns according to latitude, altitude and local time (left: Earth; right: Venus).

- **Super-rotational retrograde zonal wind (RZW)** - flowing in quasi-laminar bands parallel to equator, between the altitudes of 60-100 km and stretching between mid-latitudes. The wind starts to build up at 10 km and amplifies with altitude, reaching a maximum at cloud tops ($\sim$ 70 km). The RZW is accompanied by a Hadley-type meridional circulation from the equator to poles and both converge to an unique polar vortex circulation. On the superrotating zonal retrograde circulation, two main large scale, non-axisymmetric features are superimposed. The four-day planetary wave at low and mid-latitudes and a polar vortex in the polar regions.

- **Sub-solar to anti-solar circulation (SS-AS)** - transporting the overheated air from high insolation regions towards the nightside radiation deficit area, above 120 km altitude (thermosphere). This air motion can be inferred through the density and temperature's contrast between day and night hemispheres.

- **Meridional circulation** - characterized by one cell (Hadley) in each hemisphere, responsible for the transport of the heat excess from low latitudes, poleward to cooler high latitudes regions. The Hadley circulation consists on average of two equator-to-pole cells, with rising air at low latitudes and subsiding air at the poles, and both converge to an unique polar vortex circulation (Suomi and Limaye, 1978). The net upward transport of angular momentum by the Hadley cells is able to maintain an excess of angular momentum in the upper atmosphere, balanced by equatorward transport by planetary waves (Gierash, 1975; Rossow, 1979). However, this Hadley circulation has not been clearly characterized observationally (Sánchez-Lavega et al., 2008) and remains very much a theoretical construct in need of quantitative support. Although, the results presented in this work (and in Machado et al. (2013)), could help to constrain the meridional wind velocities.

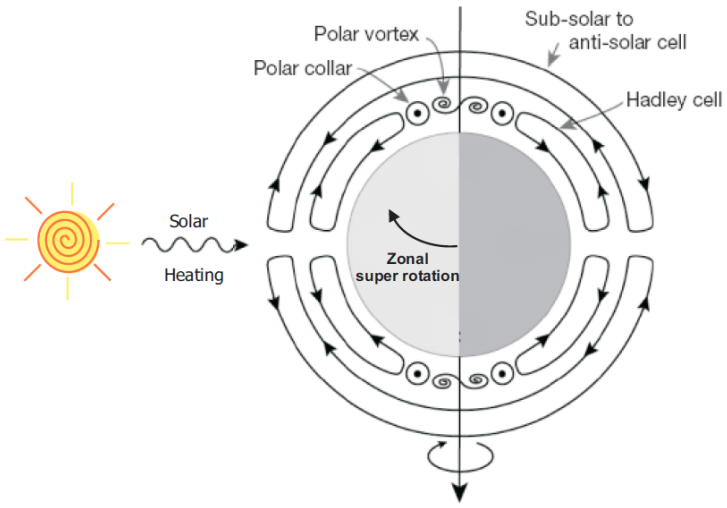

Figure 1.4: Venus atmosphere's global circulation. Figure: Taylor and Grinspoon (2009).

Polar Vortex

At polar regions, North and South, spreads a huge hurricane type structure, that surpasses in size the terrestrial major hurricanes by a factor of four (see figure 1.5 for a comparison). This three dimensional feature is highly variable, and has been seen as dipole-like shape (Pioneer Venus observations)

although it can change rapidly. The vortex eye rotates around the polar axis even faster than the super-rotating zonal winds of the mid latitudes range. The south pole vortex was observed recently (Luz et al., 2011; Garate-Lopez et al., 2013) showing a period of about 2.7 terrestrial days (twice the angular velocity of the zonal wind) and an astonishing shape variability. The inner and outer part of the vortex evidenced a differential rotation rate (Luz et al., 2011). It had been observed as a dipole, triple and monopole as well (Taylor and Grinspoon, 2009; Luz et al., 2011; Garate-Lopez et al., 2013). It remains to establish a relationship between the superrotation of the atmosphere and this phenomena, and this question is still a major theme in current scientific research.

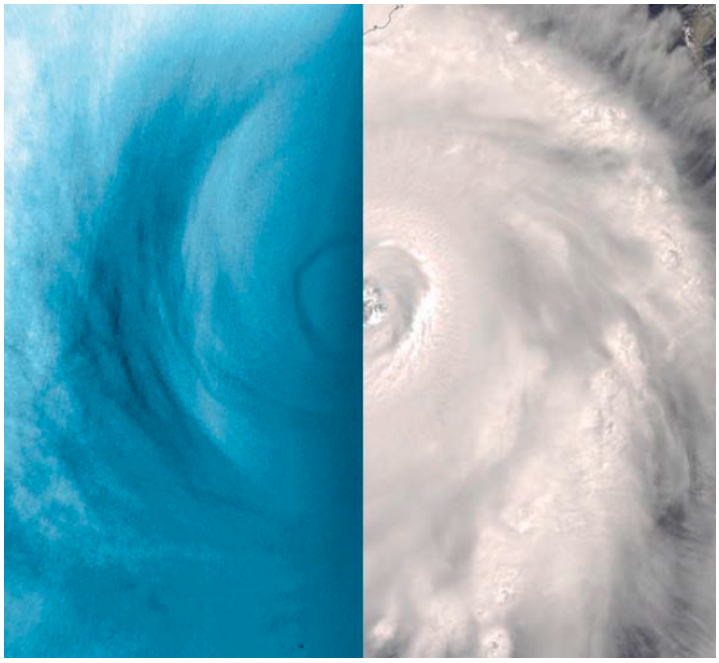

Figure 1.5: South pole vortex and comparison with a terrestrial hurricane. Figure: Limaye et al. (2009).

An intriguing VEx discovery was the presence of an atmospheric circumpolar cold zone, the cold collar (Piccioni et al., 2007). The “cold collar” (or “polar collar”) scturture appears to be a permanent structure (as is the vortex) all around the vortex, located between 60°and 70°latitude (both hemisperes). Although these structures have been observed in numerous previous observations, the formation mechanism is still unknown.

Jets and wind variability

The previous measurements by Pioneer Venus, reanalyzed in Limaye et al. (2007), showed the presence of high latitude zonal jets close to 50°latitude in both hemispheres, with a slight asymmetry between the northern and southern ones. However, long temporal averages of cloud-tracked winds by the Galileo SSI instrument (Peralta et al., 2007), and by the Venus Express VMC and VIRTIS instruments (Sánchez-Lavega et al., 2008; Moissl et al., 2009) do not display any clear evidence for high latitude jets at cloud tops, although shorter time scale averages of VMC measurements in Moissl et al. (2009) indicate that jets may occur but are short-lived. The latitudinal wind profile retrieved by Doppler velocimetry (Machado et al., 2012) and from cloud tracking methods (Moissl et al., 2009; Sánchez-Lavega et al., 2008) coincide in the presence of a jet with an increased velocity of the order of 20 m/s at the latitudes of 50-60 °. Rather than being discrepant, different wind measurements have provided important insight into the variability inherent to the circulation of Venus. In this work, direct measurements of instantaneous zonal winds brings additional evidence for the occasional presence of jets and, in general, for variability.

Vertical temperature profile

In an atmosphere in equilibrium, the weight at each atmospheric layer will be balanced by the air pressure, which results in the *hydrostatic equilibrium* equation ($\frac{\partial p}{\partial z} = -\varrho \times g$). This equilibrium leads to a vertical stratification of the atmosphere, where the pressure and the density decreases exponentially with height ($p = p_o \times e^{-z/H}$, H is the scale height).

The variation of temperature with altitude divides Venus' atmosphere into three distinct layers:

- *troposphere* (0-65 km) Extends to the top of the cloud and where the temperature decreases with altitude with the thermal gradient ratio of about $9K \cdot km^{-1}$ (close to the adiabatic lapse rate: $\Gamma_d = \frac{g}{C_p} = 7.39K \cdot km^{-1}$, which shows that convection is not significant at this atmosphere region).

- *mesosphere* (65-110 km) It is characterized by a less pronounced vertical thermal gradient ($\Gamma = \frac{\partial T}{\partial z}$) (Ahrens, 2003), being noteworthy the relevant horizontal variability with latitude, increasing from the equator to the poles, which is consistent with the existence of a Hadley circulation cell (Taylor et al., 1980).

- *termosphere* (110-200 km) The balance between the incident UV radiation and the thermal conductivity of the present molecules prevails. Here, there is an asymmetry between the day and night hemispheres, as the daytime temperature tends to increase with altitude between 100 and 140 km, while at night it tends to decrease along the same altitudes range, higher than 140 km the temperatures, at both hemispheres, remain stable, see figure 1.6.

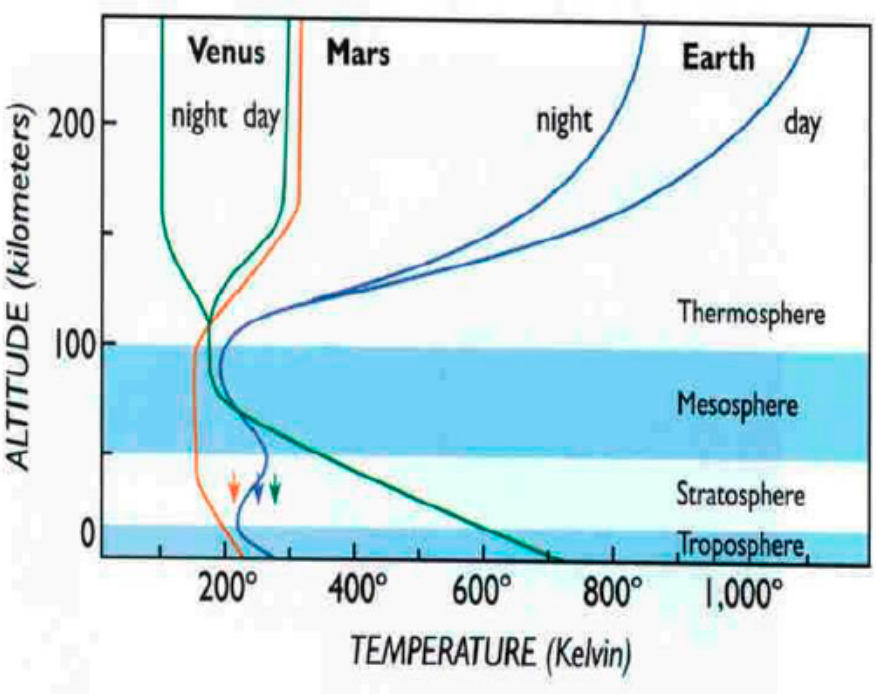

Figure 1.6: Vertical temperature profile of Venus' atmopshere (green lines), compared with Mars' (red line) and Earth's (blue lines) thermal profiles. Venus' and Earth's profiles are represented for both day and night. (image from B. Jakovsky).

Most of the unidentified UV absorber abundance is at the cloud layer and it is the responsible for about half of the total absorbed energy from solar irradiation. Allied to this fact, due to the scattering, the radiation has longer paths which increase the efficiency of solar absorption. So the cloud medium, that extends from 40 mbar (cloud top) till 1bar (cloud base), see figure 1.7, absorbs roughly 92% of the incident solar flux (that it is not reflected back

to space, due to the high reflective albedo ($\sim$ 2.5 the terrestrial one)) and just the remaining 8% will reach the surface (totally different from Earth's case). By the above, it is clear that the cloud layer (and the UV absorber) is of major importance for the atmospheric energy balance.

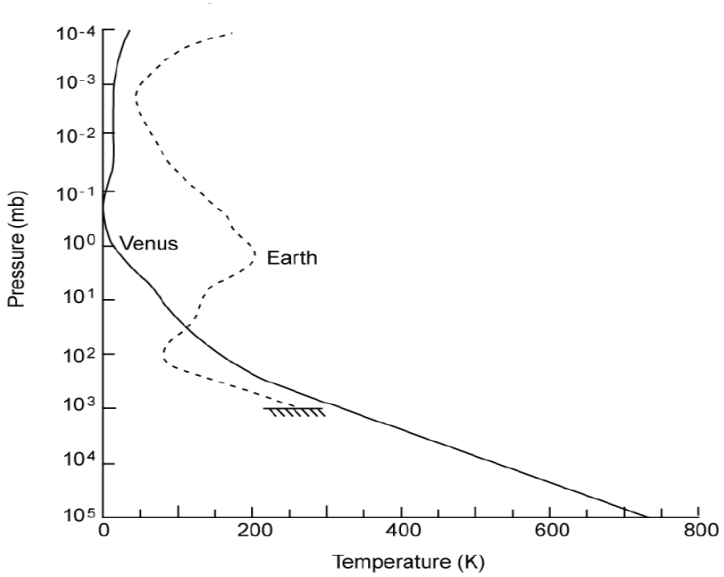

Figure 1.7: Temperature versus atmospheric pressure at Venus and Earth. Figure: (Taylor and Grinspoon, 2009)

The mesosphere shows some unexpected features, such as the latitudinal increase of temperatures from equator to poles ("warm polar" mesosphere), above 70 km of altitude. This is odd, since solar heating is higher at low latitudes than at polar region. This peculiar temperature behaviour might be due to atmospheric dynamics, and a possible cause would be a Hadley cell poleward branch that transports to high latitudes the equatorial excess of solar heating. Another curious temperature variation effect lies in the so called "cold collar", at the heights of about 65 km, characterized by a temperature decrease from equator till approximately 65° latitude, of around 25 K (Taylor et al., 1983; Piccioni et al., 2007). As a consequence of the high carbon dioxide abundance in the atmosphere which is quite efficient radiating thermal energy, in the thermosphere, above 140 km, temperature's profile remains nearly constant ($\sim$ 300 K).

A radiative transfer model utilising data from Venera 11 and Pioneer Venus missions of cloud structure, composition, temperature measurements, was developed by Pollack et al. (1980). This model introduced, as well, the SO_2, CO and HCl as sources of infrared opacity, as well as water vapour

and carbon dioxide. With these improvements, with respect to previous attempts, it was possible to accurately reproduce the observed high surface temperatures.

1.2.3 Cloud deck

The clouds on Venus have a determining influence on the planet's albedo, thermal structure and atmospheric energy balance. The cloud layer that covers the planet consists of sulphuric acid droplets (in 85% water solution) and some other aerosols of an yet unknown composition. The rapid retrograde motion of the cloud top cover is visible, through the time evolution of rapid retrograde patterns.

The cloud layer extends in the atmosphere from 48 km to 70 km (about 22 km thick), with tenuous hazes above (reaching 90 km) and below the main cloud deck (from roughly 30 km) (Esposito et al., 1983). The clouds are not homogenous regarding the average size of their aerosol particles. The cloud deck can be divided into three layers (Knollenberg and Hunten, 1980):

- **Upper layer** - Altitude between 57-68 km with an averaged particle radius of 0.3 μm, and a total optical depth of 7 at 0.63 μm;
- **Middle layer** - From 51 till 56 km altitude, with a predominance of 1-1.4 μm particle sizes, with an optical depth of about 9, at same wavelength (0.63 μm);
- **Lower layer** - The lower cloud extends from the cloud base at 48 km till 50 km, optical depth of nearly 10 (at 0.63 μm), due essentially to 3.65 μm size particles.

Polarimetric and spectroscopic observations point to a general composition ratio of one quarter of H_2O and three quarters of H_2SO_4 in the cloud particles. The atmospheric formation of sulphuric acid, near the cloud tops, comes from a photolysis and recombination processes of H_2O and SO_2 that reacts with the CO_2 following the reaction chain:

$$CO_2 + SO_2 + h\mu \longrightarrow CO + SO_3 \tag{1.1}$$

$$SO_3 + H_2O \longrightarrow H_2SO_4 \tag{1.2}$$

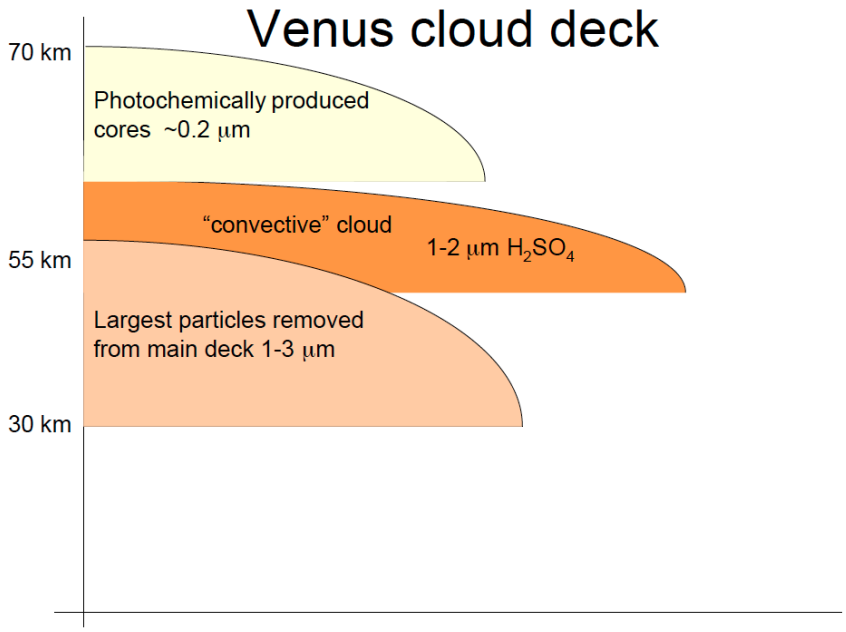

Figure 1.8: Venus' sulphuric acid cloud deck and hazes extension in altitude. Regarding the averaged aerosol particles size, the cloud deck can be divided in the three layers shown in this scheme. Figure: Titov, D., private communication.

1.2.4 Comparative climatology

Coriolis effect on Earth

Coriolis effect (named after Gaspard de Coriolis, 1792-1843) is a consequence of the principle of conservation of angular momentum. The Coriolis or geostrophic force is an apparent or hypothetical force that only acts when air is moving. A particle of air (or water), on either hemispheres, rotates from west to east with the Earth's surface at a certain speed. If that particle of air starts to move towards the equator, the conservation principle requires that the particle continue to rotate eastward at the same speed. However, the rotational speed of the Earth' surface at the equator is higher than at the poles. Thus, air moving towards the equator is deflected westward relative to the Earth's surface, while air moving from low latitudes to high latitudes (away from the equator) is deflected eastward. The *Coriolis effect* is stronger at the poles (high latitudes) and is negligible near the equator.

Cyclostrophic or geostrophic balance

The measurements of the Venus' wind velocity profile show a structure approximate to the cyclostrophic equilibrium, which postulates the balance between the pressure gradient force and the centrifugal force at a certain atmospheric layer (at fixed height). In slowly rotating bodies (such as Venus or Titan, the largest Saturn's moon), the Coriolis term will be negligible. This leads to the appearance of a wind's zonal flow, parallel to equator. In contrast to this case, we have the geostrophic balance, the one established on Earth, where the Coriolis force has an essential role in the genesis of the well known cyclonic and anticyclonic structures and their macro structures of the prevailing winds, such as the trade winds or the westerlies. In the Earth's case (and Mars), the Coriolis force overlaps the centrifugal effect due to the higher Earth's rotational velocity.

1.3 Earth's false twin: summary

As mentioned before, to understand planetary evolution, particularly in our solar system, it's essential to understand why is Venus, a planet so close and so similar (at first glance) to our Earth, so different and apparently hostile to our specie. After describing the dynamics and characteristics of Venus and its atmosphere, we can now summarize the major differences between Venus and Earth.

- Obliquity - 23° obliquity for Earth's axis, while Venus has the axis reversed and almost normal to the ecliptic (3°), resulting in non-existing seasons.
- Natural satellites - also noteworthy is the rotation stabilising influence of a terrestrial satellite (the Moon) while there is none on Venus.
- Rotation rate - Earth's rotation rate is much faster than Venus (243 terrestrial days), plus a retrograde Venusian motion
- Solar constant - Venus solar constant is almost the double relatively to the Earth's one.
- Surface temperature - a runaway greenhouse effect on Venus (due to a CO_2 dominated atmosphere) and a much lower one on Earth, contribute to a surface temperature of 460° C and 15° C, respectively.
- Surface pressure - the much denser atmosphere of Venus causes a surface pressure of 92 times the atmospheric pressure at Earth's surface.
- Water presence - water vapor and oceans on Earth, in contrast with the almost absence of water on Venus.
- Plaque tectonics - the terrestrial volcanism and the plate tectonics, by opposition of the single-plated Venus and its specific volcanism (described in section 1.1), also related with the absence of water.
- Magnetic field - Earth has an internal magnetic field and correlated "protective" magnetosphere on Earth, whereas on Venus there is just a weak induced magnetic field (see section 1.1).
- Atmosphere composition and consensable - Earth's atmosphere is mainly composed by N_2 (78%) and O_2 (20%) with water vapor as condensable, contrasting with the CO_2 (96%) dominated Venus' atmosphere with sulphuric acid H_2SO_4 as condensable.
- Atmospheric equilibrium - the rotation rate is directly related to the atmospheric geostrophic balance for the fast rotating planets (Earth and Mars) and cyclostrophic equilibrium in the slower ones (Venus and Titan).
- Atmospheric dynamics - while on Earth there is a triple cell mechanism for the meridional wind circulation, on Venus, there is a single Hadley cell in each hemisphere extending from the equatorial region to the polar region (see section 1.2.2)

1.4 Venus exploration

Venus is usually the third brightest celestial body in the sky after the Sun and the Moon (reaching the magnitude of -4.6). Given the small angular distance that separates the Sun from Venus as seen from Earth, it is seen as a "morning star" or "evening star", depending if appearing in the twilight that precedes the sunrise, or after sunset.

At the dawn of the modern age, in the year of 1610, Galileo Galilei started pointing his refractor towards Venus. He was the first man observing the phases of Venus, which became a decisive argument to support the heliocentric theory (proposed initialy by Copernicus).

Astronomical observations of Venus by Cassini and Schroter (respectively centuries 17^{th} and 18^{th}) were the first attempts to determine the plane's rotational period, both advanced with the hypothesis that it was similar to the Earth case. However, it was only in 1890 that Schiaparelli proposed a much slower rotation velocity to Venus.

1.4.1 History of spacecraft missions

More than 30 spacecraft have been launched to date toward Venus, since the beginning of robotic space exploration.

The first attempts to launch robotic probes to Venus were made in February 1961, by the USSR (Union of Soviet Socialist Republics) missions *Sputnik 7* and *Venera 1*, but they resulted in failures. The first successful flyby was carried out by *Mariner 2* (NASA) in December 1962. The images sent by the probe were a disappointment because it revealed only an opaque atmosphere that shrouded entirely the planet, like a veil that hid the planet's surface.

- Venera missions (1961-1984)

  From the mid-1960's the *Venera* probes experienced greater success. They plunged through the dense atmosphere towards the ground, but the hostile environment had been underestimated and the high pressures and high temperatures eventually crushed the first devices soon after their landing. Only *Venera 7* (August 1970) was able to achieve the desired goal of reaching the surface and send some data back to Earth. For those who expected a pleasant environment and, eventually, could support life, this was the stroke of mercy, as the readings indicated surface pressures of the order of hundred times the terrestrial atmospheric pressure (≈ 90 bars)and ground temperatures around 460°C (≈ 735 K)

The Venera program collected the first images from the surface (figure 1.9), gathering information about and surface physical and chemical conditions. Venera missions (4 to 7) confirmed the existence of an atmospheric super-rotation (Dollfus et al., 1975b).

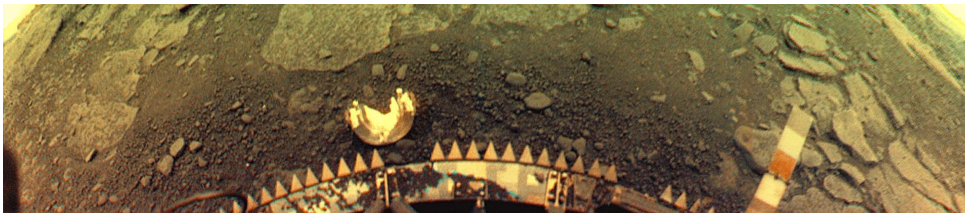

Figure 1.9: Surface photographs from the Soviet *Venera 13* spacecraft (lander touched down on 3 March 1982). The first of the Venera missions to include a color TV camera (image:: Soviet Planetary Exploration Program).

- Mariner program (1962-1973)

  The Mariner program consisted of ten exploration probes launched between 1962 and 1973. The spacecraft were designed by NASA's Jet Propulsion Laboratory to investigate the planets Mars (*Mariner 3, 4, 6, 7, 8 and 9*), Venus (*Mariner 1, 2, 5 and 10*), and Mercury (*Mariner 10*). Because of reliability issues with available launchers, the missions tended to use pairs of spacecraft launched on separate rockets. Ultimately three Mariner missions (1, 3 and 8) failed due to launch vehicle or payload shroud failures. In each case, the duplicate spacecraft was able to complete the mission (2, 4 and 9, recpectively).

  Mariner spacecrafts accomplished a number of important firsts, including the first mission to visit Venus (*Mariner 2*), the first successful Mars encounter (*Mariner 4*), and the first mission to visit Mercury (*Mariner 10*). *Mariner 10* was also the first spacecraft to visit two planets (Venus and Mercury).

- Pioneer mission (1978-1992)

  The NASA Pioneer Venus mission (not to be mistake by the *Pioneer 10 and 11*, which were launched on 1972 to study Saturn and the outer solar system) consisted of two components, launched separately: an Orbiter and a Multiprobe. The orbiter and multi-probe Pioneer Venus mission was launched in 1978. These probes made an invaluable contribution for the study of this planet, mapping the planetary surface by radar. Its high elliptical orbit allowed a global mapping of the cloud deck, ionosphere, upper atmosphere, surface radar-mapping, among

other experiments. The descent probes deployed, in turn, carried two experiments, a neutral mass spectrometer and an ion mass spectrometer to study the composition of the atmosphere. The performed measurements of cloud and atmospheric characteristics were essential in the construction of Venus atmospheric models (Colin and Hunten, 1977).

The Pioneer project was responsible for the first measurements of the weak magnetic field of Venus, by means of its onboard magnetometer readings, which was confirmed by later observations from ESA's Venus Express. This magnetic field is the result of the interaction of the solar wind with the ionosphere (not due to the planetary dynamo's model). PV also produced the first indirect measurements of mesospheric winds, estimated by observing the UV cloud tops markings. This mission was also responsible for the discovery of the vast double vortex at the northern polar region.

On 8 October 1992, as its fuel supply exhausted, the Orbiter ended its mission as a meteor flaming through the dense atmosphere of Venus.

- Vega mission (1984-1985)

  The new soviet mission was the natural continuation of the previous Venera program. This spacecraft mission combined a Venus swingby and a Comet Halley flyby. Two identical spacecraft, *Vega 1* and *Vega 2*, were launched December 15 and 21, 1984, respectively. The mission used the same basic probe and landers design, but now also with atmospheric balloons, that could survive longer than the landers and in the meanwhile measured the pressure, temperature and even the wind velocity (Blamont, 2008). After carrying Venus entry probes to the vicinity of Venus , the two spacecraft were retargetted using Venus gravity field assistance to intercept Comet Halley in March 1986.

  The Vega and Pioneer missions were essential for the structured study of the atmospheric chemical behaviour and physical description. Their measurements showed the evidence of an extremely active atmosphere, containing corrosive gases and a thick cloud layer.

- Magellan (1989-1994)

  The Magellan spacecraft, named after the sixteenth-century Portuguese explorer (*Fernão de Magalhães*) whose expedition first circumnavigated the Earth, was launched 4 May 1989, and arrived at Venus on 10 August 1990. Magellan collected radar images of 98 percent of the planet's surface, with resolution (of around 200 meters) 10 times better than that of the earlier Soviet Venera 15 and 16 missions. Altimetry and

radiometry data also measured the surface topography and electrical characteristics. When it reached the end of its extended mission, in 1994, the probe was control-crashed into the planet with the objective of obtaining some final atmospheric data along the descent (Saunders et al., 1992).

- Galileo (1989-2003)

  The Galileo spacecraft made a Venus fly-by gravity assisted maneuverer on its way to Jupiter. The observations made during closest approach took advantage of its high resolution infrared camera. The images taken at that time contributed to improve the knowledge about cloud properties and their variability (Carlson et al., 1993). Galileo Near Infrared Mapping Spectrometer (NIMS) made night-side observations of the atmosphere's infrared emission at 2.3 μm. This instrument took advantage of the carbon dioxide and water vapour opacity wavelength window through 2.1-2.6 μm. The region probed at this specific wavelength (2.3 μm) is from below the cloud deck.

  Galileo made flybys to Venus, Earth and the moon, before reaching as far out in the solar system as the asteroid belt, enabling the first close-up studies of two asteroids, *Gaspra* and *Ida*. Additionally, in 1994, Galileo scientists were fortunate to be the only ones with a direct view of the Comet Shoemaker-Levy 9 fragment impacts on Jupiter. All of this was prior to the primary missions of sending an atmospheric probe into Jupiter's atmosphere and studying Jupiter, its satellites, and its magnetosphere for two years with the orbiter. Galileo ceased operations and it was plunged into Jupiter's crushing atmosphere on Sept. 21, 2003

- Flybys

  Cassini (1997-...) The Cassini/Huygens' mission is defined in broad terms as a detailed study of Saturn, its rings, icy satellites, magnetosphere, and Titan. Cassini completed its initial four-year mission to explore the Saturn System in June 2008 and the first extended mission, in September 2010. Now, the healthy spacecraft is seeking to make exciting new discoveries in a second extended mission. This mission's extension is planned to go through September 2017. Four flybys of planets – two of Venus and one each of Earth and Jupiter – gave Cassini the speed it needed to reach Saturn. Cassini first flew past Venus on April 26, 1998, and also on June 24, 1999.

Messenger (2004-...) The Mercury Surface, Space Environment, Geochemistry and Ranging (MESSENGER) mission was designed to study the characteristics and environment of Mercury from orbit. The spacecraft flew past Venus on October 24, 2006 and June 5, 2007.

1.4.2 Venus Express

Overview

After a long pause (about a quarter of a century) in spacecraft exploration of Venus, the European Space Agency (ESA), launched on November 9, 2005 (it arrived at Venus in April 2006) its first Venus exploration mission, Venus Express (VEx) spacecraft with the task of conducting studies under the general circulation of the atmosphere, the chemistry of clouds and the atmospheric escape processes of several different volatiles, as well as the interactions between the surface and the atmosphere, with emphasis on the Venusian volcanism.

The orbital period was of 24 hours. The orbital design was elliptical, highly eccentric, with a planetary close pericentre of 250 km and an apocentre of 66 000 km. This orbit configuration provided optimal coverage of planetary latitudes and solar local time. The highly elliptic orbit allows global large scale investigations, as high spatial resolution detailed studies of localized phenomena, at pericentric close approach.

After eight years in orbit and with propellant for its propulsion system running low, Venus Express was tasked in mid-2014 with a daring aerobraking campaign, during which it dipped progressively lower into the atmosphere on its closest approaches to the planet. This unique adventure was aimed at reducing the altitude and allowing an exploration of previously uncharted regions of the atmosphere. The lowest point of the orbit was gradually reduced to about 130-135 km altitude. The campaign also provided important experience for future missions - aerobraking can be used to enter orbit around planets with atmospheres without having to carry quite so much propellant. During an orbit maneuver to raise the spacecraft's altitude in the hopes of extending the mission's lifetime, the spacecraft's remaining fuel was exhausted and the contact with the spacecraft was lost on November 28, 2014. The mission was officially declared over by ESA on December 16, 2014.

Instruments

In this section we present a resume of the instruments aboard VEx orbiter. The results presented in this work were obatined through coordinated

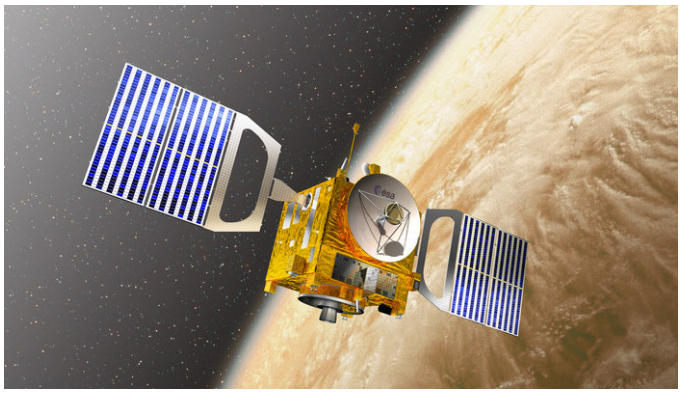

Figure 1.10: Artist's view of Venus Express probe in orbit around Venus (image: ESA's Venus Express mission website).

observations between gound-based telescope (CFHT/ESPaDOnS) and space observations (VEx/VIRTIS). Figure 1.11 illustrates the size and location of instruments on the spacecraft.

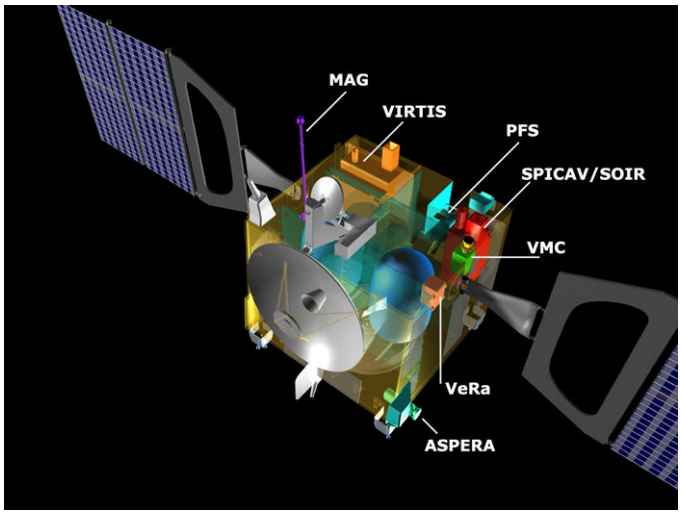

Figure 1.11: A cutaway diagram showing size and locations of Venus Express instruments: MAG, VIRTIS, PFS, SPICAM/SOIR, VMC, VeRa and ASPERA.

- MAG (Venus Express Magnetometer). Venus has no detectable internal magnetic field, and the field that exists around the planet is entirely due to the interaction between the solar wind and the atmosphere. The MAG magnetometer studied this process and contributed to the

understanding the effect this has on Venus' atmosphere, for instance the atmospheric escape process.

- VIRTIS (Visible and Infrared Thermal Imaging Spectrometer) was able to study the composition of the lower atmosphere between 40 km altitude and the surface. It tracked the clouds in both ultraviolet and infrared wavelengths and allowed scientists to study atmospheric dynamics at different altitudes. This cloud-tracking technique was used in coordinated observations with our ground-based Doppler velocimetry, allowing for comparative a study of wind velocities at 70km altitude. The instrument combines a double capability: a high-resolution imaging in the visible-infrared range (0.28-5 μm) at moderate spectral resolution (VIRTIS-M channel) and a high-resolution spectroscopy in the 2-5 μm range (VIRTIS-H channel). The scientific objectives of VIRTIS cover a large field and span from the study of the thermal emission of the surface up to the composition and dynamics of the upper atmosphere.

- PFS (Planetary Fourier Spectrometer) was able to measure the temperature of the atmosphere between altitudes of 55-100 km at a very high resolution. It was also be able to measure the surface temperature and therefore be able to search for volcanic activity. In addition to its temperature measurements, PFS made composition measurements of the atmosphere.

- SPICAV/SOIR (Ultraviolet and Infrared Atmospheric Spectrometer) was designed to assist in the analysis of Venus' atmosphere. In particular, searching for the small quantities of water expected to exist in the Venusian atmosphere, looking for sulphur compounds and molecular oxygen in the atmosphere and determining the density and temperature of the atmosphere at 80-180 km altitude.

- VMC (Venus Monitoring Camera) is a wide-angle multi-channel camera that was able to take images of the planet in the near infrared, ultraviolet and visible wavelengths. VMC was able to make global images and studied the cloud dynamics and image the surface. In addition it assisted in the identification of phenomena seen by other instruments.

- VeRa (Venus Radio Science Experiment) used the powerful radio link between the spacecraft and Earth to investigate the conditions prevalent in the ionosphere of Venus. Scientists used it to study the density, temperature, and pressure of the atmosphere from 35-40 km up to 100

km from the surface, and to determine roughness and electrical properties of the surface. It also allowed investigations of the conditions of the solar wind in the inner part of the Solar System.

- ASPERA (Analyser of Space Plasma and Energetic Atoms) was designed to investigate the interaction between the solar wind and the atmosphere of Venus by measuring outflowing particles from the planet's atmosphere and the particles making up the solar wind. It studied how the molecules and ions escape the planet.

Scientific discoveries

In this section we present a resume of the most relevant scientific contributions made by VEx.

- Super-rotation speed variability

  By tracking the movements of distinct cloud features in the cloud tops some 70 km above the planet's surface over a period of 10 Venusian years (6 Earth years), scientists were able to monitor patterns in the long-term global wind speeds.

  In 2006, average cloud-top wind speeds between latitudes 50°on either side of the equator were clocked at roughly 300 km/h. However, these already rapid winds are becoming even faster, increasing to 400 km/h over the course of the mission.

  There have also been dramatic variations in the average wind speeds observed between consecutive orbits of Venus Express around the planet. In some cases, wind speeds at low latitudes varied such that clouds completed one journey around the planet in 3.9 days, while on other occasions they took 5.3 days.

- Shape-shifting polar vortices

  The new observations show that the center of the vortex has a highly variable shape and internal structure, and its morphology is constantly changing on timescales of less than 24 hours, as a result of differential rotation. These rapid shape changes indicate complex weather patterns, which are strongly influenced by the fact that the center of the vortex does not coincide with the geographical pole.

  The center of rotation drifts right around the pole over a period of 5-10 Earth days. Its average displacement from the South Pole is about three degrees of latitude, or several hundred kilometers. Although its

highly elliptical orbit means that Venus Express flies too close to the planet's North Pole for detailed imaging, it is likely that both vortices have similar structures and behave in a similar way.

- Water loss

  Venus Express has confirmed that a large quantity of water has been lost into space over billions of years. The spacecraft's magnetometer instrument (MAG) made the first ever detection of atmospheric loss on Venus' day side. Then, in 2007, the Analyzer of Space Plasma and Energetic Atoms (ASPERA) instrument discovered a rapid loss of hydrogen and oxygen from the night side. This depletion occurs because water molecules in its upper atmosphere are split by incoming ultraviolet radiation from the Sun. This process creates two hydrogen atoms and one oxygen atom for each dissociated molecule. The solar wind - a stream of charged particles from the Sun - then strikes the upper atmosphere and carries the hydrogen and oxygen atoms into space. Unlike Earth, Venus does not generate a magnetic field which can protect its atmosphere from the solar wind. Venus Express has measured the rate of this escape and confirmed that roughly twice as much hydrogen as oxygen is escaping, confirmation that water (H_2O) is the source of these escaping ions. It has also shown that a heavy form of hydrogen, called deuterium, is progressively enriched in the upper regions of Venus' atmosphere because the heavier gas finds it less easy to escape the planet's gravitational grip.

- Ozone layer

  According to the new data, ozone is located at varying altitudes in the Venusian atmosphere, between 90 and 120 km (compared with 15-50 km on Earth) and is always confined to a rather thin layer, measuring 5 to 10 km across. The ozone layer on Venus is also very tenuous - up to 1000 times less dense than that on Earth. One surprise was the absence of ozone at the anti-solar point, where molecular oxygen is highly concentrated. Oxygen atoms transported to the anti-solar point give rise to molecular oxygen, so some production of ozone was also expected. However, none was found. The lack of ozone detected there can be explained if the molecules are destroyed by chlorine-based compounds, which are funnelled to the anti-solar point by the same mechanism that carries the oxygen there. The chlorine-catalyzed destruction of ozone at Venus' anti-solar point may be caused by reactions very similar to those responsible for the Antarctic 'ozone hole' on Earth, highlighting the similarity of atmospheric processes on these two planets.

- Magentosphere

  Although Venus has no magnetosphere to deflect the charged particles of the solar wind (electrons and protons) as they stream past the planet, it is partially protected from erosion of the outer atmosphere by an induced magnetic field arising from the interaction of the solar wind and the planet's ionosphere.

  As on Earth, solar ultraviolet radiation removes electrons from the atoms and molecules in the upper atmosphere, creating a region of electrically charged gas known as the ionosphere. This ionised layer interacts with the solar wind and the magnetic field carried by the solar wind, diverting the flow of particles around the planet, creating an elongated magnetotail, on the lee side of the planet.

  At Earth, the process occurs at a distance of about 10-30 planetary radii down the magnetotail. Since Earth's magnetosphere is 10 times larger, reconnection at Venus would be expected to occur 1-3 radii down its tail - precisely where Venus Express detected the reconnection events.

Coordinated observations (ground and space)

The coordinated observations between ground-based telescopes and space probes (with Venus Express) provided consistent and relevant results and proved to be a key factor in studying many important aspects of Venus' atmosphere, as is the measure of wind velocity in the cloud top. The work developed in collaboration with VEx, and its success, paved the way for future collaborations with space missions, as we expect to be case of Akatsuki.

1.4.3 Akatsuki

The AKATSUKI spacecraft was launched in May 2010. After its smooth flight, JAXA attempted to insert the orbiter into the orbit circling around Venus on Dec. 7, 2010, but it failed as the main engine for orbit control was broken. JAXA established an investigation team to find the cause of the failure while studying a feasible plan for a second attempt. The spacecraft - whose name means "Dawn" in Japanese - had been circling the sun for five years, waiting for another shot at Venus. On Dec. 7, 2015, JAXA successfully inserted the orbiter into the Venus orbit by emitting thrust from the attitude control engine.

Akatsuki's current path takes it as close as 400 km to Venus, and as far away as 440 000 km. This orbit is much more elliptical than the one Akatsuki

was supposed to achieve in 2010, which featured a period of 30 hours and an apoapsis (most distant point from Venus) of about 80 000 km.

Akatsuki is the second interplanetary mission in Japan's history. The country's first, the Nozomi Mars probe, failed to arrive as planned at Mars in 2003. In 2007, Japan's Kaguya orbiter successfully launched to the moon to study the lunar surface from orbit. Kaguya's mission ended in 2009 and it ultimately crashed into the moon's surface.

Coordinated observations between ground-based and Akatsuki probe were made in January 2016, in order to study and measure wind velocity at could top of Venus' atmosphere, using both could-tracking (Akatsuki) and Doppler velocimetry (CFHT/ESPaDOnS). The previous ground and space coordinated observations with VEx granted our team experience and expertise that should contribute for the success of the current Akatsuki collaboration.

Chapter 2

Methods: Doppler Velocimetry and Cloud Tracking

2.1 Doppler velocimetry

The main purpose of this study is to provide direct wind velocity measurements using visible Fraunhofer lines scattered by Venus' cloud tops. The solar Fraunhofer spectrum results from absorption of continuum radiation emitted from warmer, deeper layers by atoms and molecules of the solar atmosphere (such as H, S, Si, Fe, Ba, Mg, CN). The sunlight is absorbed by the particles in Venus' top clouds and re-emited in Earth's direction (in a single scatter approximation).

The methods developed in recent planetary wind measurements in the visible range using high-resolution spectroscopy (Civeit et al., 2005; Luz et al., 2005a, 2006; Widemann et al., 2007, 2008) address the fundamental problem of maintaining a stable velocity reference. There are systematic errors involved in trying to measure absolute wavelengths or Doppler shifts with grating spectrographs, simply because the dispersion law and instrumental uncertainties, for simple line shifts, cannot achieve an absolute accuracy better than about 100 m/s. In measuring the global wind circulation at cloud tops, we are addressing wind amplitude variations or wind latitudinal gradients on Venus of the order of 5-10 m/s projected on the line-of-sight. In order to overcome this problem, the Doppler measurement is based on an optimal weighting of the Doppler shifts of all the lines present in the spectrum, with relation to a reference spectrum (in this case, a Th-Ar spectrum, obtained through a exposure lamp).

The Doppler velocimetry method used in this work was developed by Dr. Thomas Widemann (Widemann et al., 2008) and Dr. Pedro Machado

(Machado et al., 2012).

2.1.1 Method Summary

In order to derive the wind radial velocity w_i at each point (along the line-of-sight) in the planetocentric frame (P), i.e. in Venus' frame, the spectral calibration and radial velocity measurement is performed in the following steps:

1. Spectral wavelength calibration performed at beginning and end of the acquisition session;
2. Since Earth's atmosphere also scatter solar radiation, the pipeline (both instrumental and user developed pipelines) identifies two peaks in the spectrum (from the solar radiation scattered by Venus' and Earth's atmospheres, tough some lines are absorbed by Earth's atmosphere) with a relative shift.
3. The Venus-scattered velocity h (in barycentric frame - B) is extracted by applying a least-squares deconvolution fit to the correlation function between Fraunhofer lines scattered at Venus and Earth's atmospheres.
4. Correction from Earth's spin and orbital motion ($berv$) and Venus' orbital motion (V_{topo}).

After obtaining the wind radial velocity w_i it's necessary to perform additional astronomical corrections in order to obtain real radial wind velocities:

5. Correction of the Young effect (the influence of an unbalanced illumination from the two limbs of the rotating Sun).
6. Correction of the instrumental spectral drift (an on-target monitoring of the instrumental spectral drift to a specific location on Venus' disk - reference point)

Since the obtained values are the line-of-sight components of the wind velocities, it's necessary to perform a final step in order to obtain the actual wind velocities vectors.

7. De-projection of the radial velocities to obtain the final zonal (parallel to the equator) and meridional (along the meridians) wind velocities.

Table 2.1 details the nomenclature used for the deprojected and modeled horizontal winds, used either in chapthers 2 (Method) and chapther 5 (Results).

Task	Measurement/calculation	output
	CFHT/ESPaDOnS line of sight/horizontal velocities :	
w_i	$h - (berv + v_{topo})$	Line-of-sight velocity in (P)
v_i	$w_{i,c} - w_{i,c,ref}$	Line-of-sight velocity, Young / ref. corr.
v'_i	$v_i - v_{i,trend}$	Line-of-sight velocity, detrended w/pt-10 exp.
$\overline{v}'_i$		Horizontal velocity at point i, day averaged
$v_{z,i}$		Zonal wind component at point i, instantaneous
$\overline{v}_z$	1-wind, v_{eq} zonal fit to $\overline{v}'_i$	Zonal wind fit, all latitudes, day averaged
$\overline{v}_m$	1-wind, v_{45° meridional fit to $\overline{v}'_i$	Meridional wind fit, HPA meridian, 2-day averaged
$\overline{v}_{z,lat}$		Zonal wind fit, latitude band *lat*, day averaged
$v_{z,lat}$		Zonal wind fit, latitude band *lat*, one sequence
	VEx/VIRTIS-M velocities :	
$v_{z,CT}$	Manual tracking of UV-dark cloud features	Cloud tracking, zonal wind component
$v_{m,CT}$	Manual tracking of UV-dark cloud features	Cloud tracking meridional wind component

Table 2.1: Velocity symbols used for deprojected and modeled horizontal winds in visible Doppler velocimetry using CFHT/ESPaDOnS data and VEx/VIRTIS cloud tracking data (two last entries). All data and fit units are m s^{-1} in Figures and Tables unless specified otherwise. Results are expressed in planetocentric frame (P).

2.1.2 Projected Radial Velocities

The Doppler shift measured in solar scattered light on Venus' day side is the result of two instantaneous motions: (1) an instantaneous motion between the Sun and Venus' upper cloud particles; this Doppler velocity is minimal near Venus sub-solar point; (2) a motion between the observer and Venus clouds, resulting from the topocentric velocity of Venus cloud particles in the observer's frame; this effect is minimal near Venus' sub-terrestrial point. These combined instantaneous motions add-up and the combined Doppler shift vary spatially as a function of the planetocentric longitude and latitude at Venus. Considering that Φ is the phase angle between the Sun and Earth, centered on the target (Venus), at $\Phi/2$ the sum of both Doppler components (the sunlight that reaches Venus, with redshift, and the light re-emitted from Venus to Earth, with blueshift) is zero (see the schematics of a single scattering approximation in figure 2.1). In other words, the particles velocities relatively to the radiation source (moving away) and relatively to the observer (moving towards) cancel each other out, resulting in an apparent null-Doppler meridian, in the case of a pure zonal wind field.

2.1.3 Fraunhofer absortion lines at Venus and Earth

Solar radiation is scattered from both Venus' and Earth's atmospheres, although some of the Fraunhofer lines are absorbed by Earth's atmosphere.

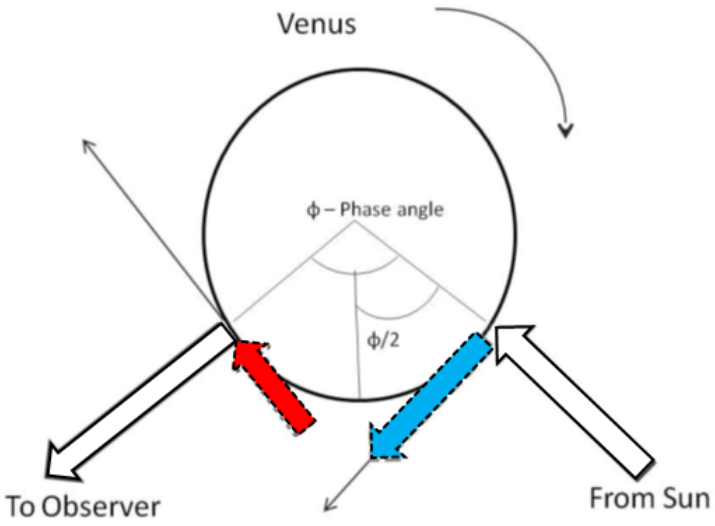

Figure 2.1: Schematics of the Doppler effect, considering a single scattering approximation. The direction of the Venus' rotations is shown by the top arrow. The solid white arrows represent radiation being absorbed (right hand side) and emitted (left hand side) without Doppler effect. Dashed arrows represent radiation being absorbed (red) or emitted (blue) with the respective Doppler effect.

The instrument registers both spectra and a least-squares deconvolution is applied to the pattern of Fraunhofer lines, using a G2 type star mask (Sun's stellar type), providing the radial velocity (along the line-of-sight) in the solar system barycentric frame (B). The Venus-scattered velocity h is extracted by applying a double-Gaussian fit to the correlation function between Fraunhofer lines at Venus and Earth ones.

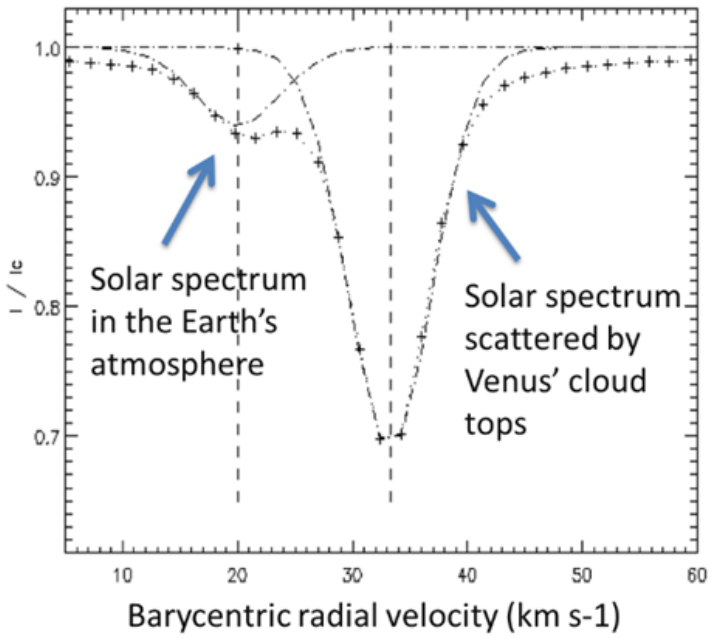

Figure 2.2: Correlation function of Fraunhofer lines scattered from Venus' and Earth's atmospheres.

2.1.4 Wind radial velocity

We derive the instantaneous Doppler shift for the motion of the cloud top aerosol particles in the planetocentric frame:

$$w_i = h - (berv + v_{topo}) \tag{2.1}$$

Where w_i is the radial component of the instantaneous velocity of Venus' top clouds in the observer's direction expressed in the Venus center rest frame (P, planetocentric), h is the absolute velocity of solar lines scattered off Venus clouds expressed in the barycentric frame (B), $berv$ is the correction from Earth's spin and orbital motion, i.e. observer's motion in the barycentric

frame (B) (provided directly by the instrument pipeline), and V_{topo} is the instantaneous velocity of Venus' center of mass in the topocentric frame (T) (which is determined with *Horizons* ephemeris provided by the Jet Propulsion Laboratory - NASA-JPL).

2.1.5 Young effect

Due to the large, 0.5°, angular size of the Sun and its fast rotation (∼2 km/s), a differential elevation of the finite solar disk near terminator will result in unbalance between the contribution of the approaching solar limb (blue shifted radiation) and the receding solar limb (red shifted radiation). In such geometry, the excess of one or the other will affect the apparent line Doppler shifts measured along the Venus atmosphere. This is called the "Young effect". It can be shown that this effect is of the order of the Sun's equatorial velocity (2 km/s), multiplied by the ratio of its apparent radius as seen from Venus, to the angular distance from the target point to the terminator, and can be empirically approximated by:

$$Y \sim \frac{V_{\odot} D_{\odot}}{\sin\theta} \tag{2.2}$$

where $V_{\odot}$ is the solar equatorial velocity (2 km/s), $D_{\odot}$ is the solar angular diameter and θ the angular distance between the point being observed and the terminator. This equation is equivalent to the empirical relation proposed by Young (1975):

$$Y = 3.2\tan(SZA) \tag{2.3}$$

where SZA is the solar zenith angle (Young, 1975). The Young effect becomes significant near the terminator (which was near the central meridian in our observations), where it increases substantially. To correct the measured Doppler shift from the Young effect, we proceeded as follows:

$$w_{i,c} = w_i + Y(\phi, \psi) \tag{2.4}$$

where $w_{i,c}$ is the projected wind velocity along the line-of-sight, w_i is the measured Doppler shift (equation 2.1, section 2.1.4) Y is the corrective term due to the Young effect, function of ϕ and ψ, the planetocentric latitude and longitude of the observed point upon the disk.

2.1.6 Instrumental spectral drift

After the instantaneous velocity of Venus center of mass v_{topo} has been subtracted, spectral wavelength calibration is performed at beginning and

end of the acquisition session by means of a Th-Ar lamp exposure. Earth's atmosphere absorption lines superimposed to Venus' spectra are used as additional on-sky velocity calibration.

Because CFHT/ESPaDOnS acquisition on Venus disk is sequential, in measuring the global wind circulation at cloud tops, we are addressing wind amplitude variations or wind latitudinal gradients on Venus of the order of 5-10 m/s projected on the line-of-sight. It is therefore necessary to measure relative Doppler shifts between two sets of absorption lines. As no absolute velocity can be retrieved on sky at an accuracy better than about 100 m/s (Widemann et al., 2008), we proceed with relative Doppler velocities by choosing arbitrarily the first spectrum of each series of sequential acquisitions $w_{i,c,ref}$ as a velocity reference, so that

$$v_i = w_{i,c} - w_{i,c,ref} \tag{2.5}$$

Figure 2.3 shows line-of-sight velocities v_i with their error bars σ_i. They are plotted as a function of time, with target point numbers superimposed. Immediately apparent is a slow drift of the point 4 velocities. This drift occurs, presumably, due to still imperfectly corrected instrumental effects and measurement of solar absorption lines with respect to telluric lines (Young et al., 1979; Widemann et al., 2007).

The spectral calibration at high resolving power (80 000) is naturally fluctuating because of several effects, such as mechanical or thermal variations in the spectrograph and its environment. To correct any spectral drift due to instrumental effects, as is the case of mechanical flexure, temperature or pressure variations in the spectrograph chamber (see section 3.2.3) or along the coudé optical path we fit the reference point 4 velocities on Venus' to a series of linear segments $v_{trend}(t)$ (dotted line on figure 2.3 bottom plot), so that:

$$v'_i = v_i - v_{i,trend} \tag{2.6}$$

This corrections requires an observation of a reference point before and after each sequence of points are observed. This way, we can measure the drift observed in the reference point and subtract it from all the measures of all the other points.

2.1.7 Error estimate

Absolute error on a given absolute velocity measurement $w_{i,c}$ results from the combination of a number of uncertainties: (i) the Th-Ar dispersion lamp spectrum uncertainty; (ii) the least-square deconvolution of Fraunhofer lines

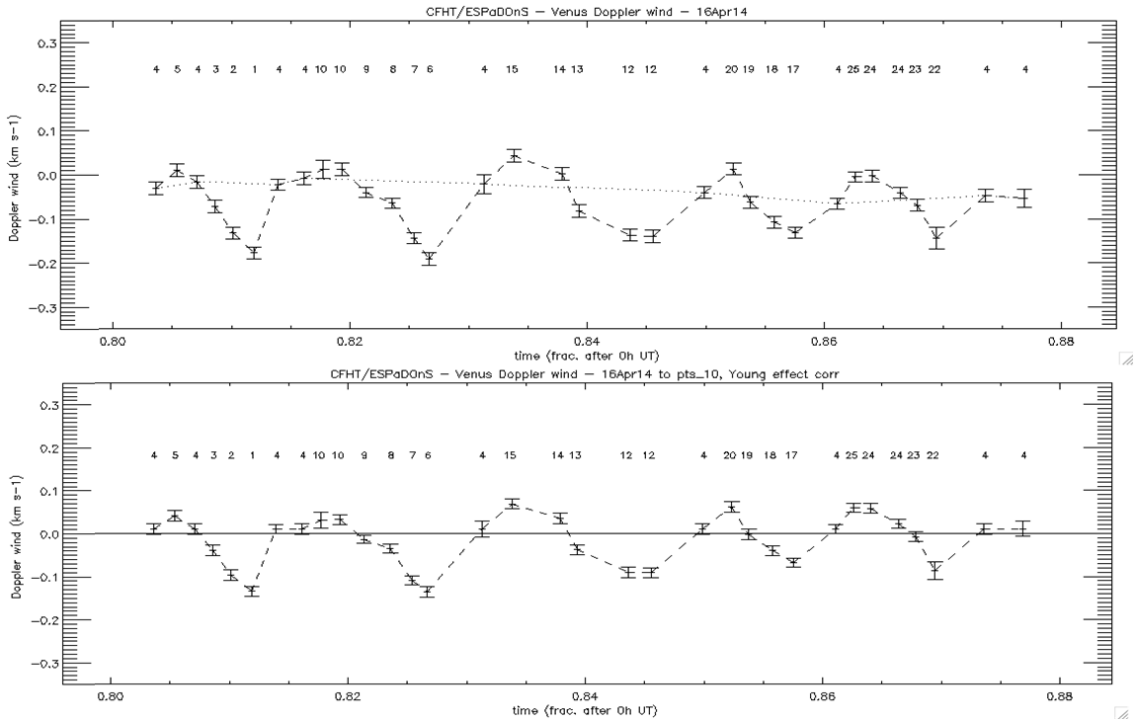

Figure 2.3: Doppler winds v_i and v_i' on April 16. Point acquisition numbers are indicated in reference to Table 4.2 and Fig.4.13. X-axis is fraction of day after 0h UT. (a) top: relative velocity $v_i = w_{i,c} - w_{i,c,ref}$. Dotted line: vtrend(t) ; (b) bottom: kinematical fit to Apr. 16 differential wind field $v' = v_i - v_{i,trend}$ corrected for Young effect, to a pure zonal circulation with v = (117.4). The trend line (top plot) signalizes the spectral drift occurring in the observational run. By fitting the trend line of the reference point values (point 4) we can correct the drift effect that affects all the other measures (bottom plot).

uncertainty; (iii) the additional fit to telluric line shift uncertainty; (iv) the errors due to additional weather conditions such as passing cirrus clouds, temperature variations or spectrograph mechanical flexure; (v) the uncertainly resulting from guiding and pointing errors during acquisition. Note that the reference trend polynomial $v_{i,trend}$ is also affected by these combined uncertainties.

Rather than trying to calculate an upper limit to the combination of the various error terms (i)-(v), we take advantage of repetition of short-time exposures at each point, to test the internal consistency of the retrieved radial velocity h. To estimate the individual error on each velocity measurement we repeated three times the short-time (3 sec) exposures at each target point and calculated the respective standard deviation (σ_i). The variability from successive exposures at each observational point indicates a high consistency, with an upper limit of 5 to 6 m/s between the mid latitudes range, but growing to twice this value at low SNR and/or higher latitudes or high SZA near terminator. Individual target point's velocities were obtained by weight-averaging the retrieved values from the consecutive exposures taken at each Venus target pointing. Considering that σ_i is the error on the point 4 velocity relative to the measurement v_i, therefore the statistical combined error at each point is given by

$$\sigma'_i = \sqrt{\sigma^2_{trend,i} + \sigma^2_i} \tag{2.7}$$

To determine $\sigma^2_{trend,i}$ on the trend fitting function $v_{i,trend}$ at each point i, we linearly interpolated the error bar along the segment between two point-4 exposures, which have been determined by taking advantage of repetition of short-time exposures.

2.1.8 Pointing accuracy

Telescope offset positions relative to disk center were calculated and guided at each point using the telescope control system (TCS) and interpolated non-sidereal drift rates. Each offset position is manually reached and guided using the telescope controls and a template of the pointing sequence dimensioned to ESPaDOnS's guiding camera display. The manual guiding on each point extends for approximately 3 min (3-s exposures followed by 40 s of readout/processing). The observer can manually correct the tracking errors during the overhead time between sky exposures. The estimated combined pointing and tracking error is less than 0.4 arcsec, of the order of seeing conditions and within the ESPaDOnS FOV projected diameter of 1.6

arcsec on Venus. Note that this upper limit is equal for all points as the quality of guiding is independent of the solar zenith angle on Venus.

2.1.9 Sensitivity tests

In order to test the robustness, reliability and sensitivity of the Doppler velocimetry algorithm used, it was performed several additional sensitivity tests.

With the aim of improving the quality and increase the confidence in the results obtained, we built fully synthetic spectra, constructed from Gaussian line shapes, to which we imposed artificial shifts corresponding to known velocities. Then we ran the algorithm to produce the respective velocity curves and compared the velocities retrieved and the imposed ones.

The tests included the modelling of fully synthetic spectra as well as modified actual observational data to which artificial Doppler shifts were imposed (from now on denominated: synthetically reconstructed spectra).

Although the tests were made based on the observations with the *Ultraviolet and Visual Echelle Spectrograph* (UVES) at the *Very Large Telescope* (VLT), the consistency of the method is directly applied to the observations made with the ESPaDOnS at the CHFT. Both observations were made with an high resolution spectrograph and both used the same Doppler velocimetry method.

Synthetically reconstructed spectra tests

With the goal of testing the behaviour of the data reduction algorithm we produced reconstructed spectra from spectra derived from actual observations. We then obtained the velocity curves for these changed spectra.

In the first test, the first step consisted of replacing all the spectra (61) by the central spectrum, to ensure a relative null velocity between each of the spectra and the reference spectrum. The algorithm retrieved null Doppler shifts, as expected. In the second test all the spectra except the reference one were shifted by a prescribed shift. The spectra were shifted with 10 m/s increments, between -300 m/s and 300 m/s from top to bottom of the slit. We then produced the velocity curves for these changed spectra. This test confirmed that the velocity curves for the reconstructed spectra were consistent with the imposed deviations (figure 2.4).

On the other hand, reconstructing the orders from a spectrum with a lower signal to noise ratio led to retrieved velocities lower than the prescribed ones (figure 2.5). The error bars were also higher for tests with spectra

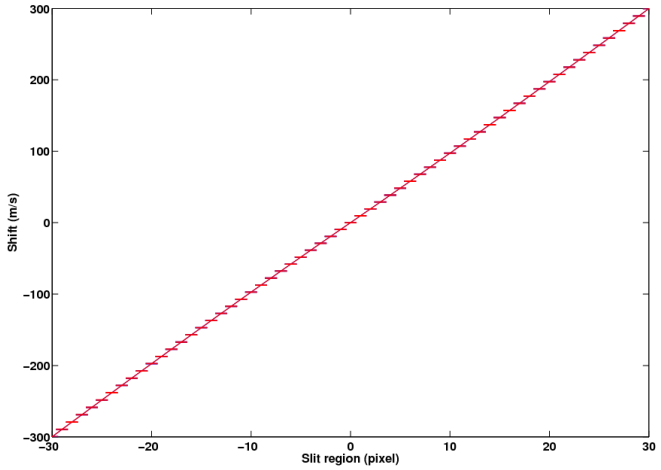

Figure 2.4: Doppler shift curve for spectra shifted with a 10 m/s step relative to the central spectrum, between -300 m/s and +300 m/s. This curve has been retrieved from a synthetic spectrum.

from the MIT detector, due to the higher noise of the observations at longer wavelengths in this observational offset (figure 2.5b).

To test the algorithm's response to wavelength range, reconstructed spectra were also produced in which only one of the spectral orders was reconstructed as previously described, while all other orders were replaced by an average of the continuum level. Since there was no significant discrepancy between velocity curves obtained from different spectral orders, we conclude that our method is robust with respect to the wavelength range of the data. This is not surprising since the density of spectral lines has little variation between spectral orders.

Fully synthetic spectra tests

These tests were based on fully synthetic spectra constructed from gaussian line shapes. The reference spectrum was constructed by defining the line width, depth and density (i.e. the average number of spectral lines per nanometer) so as to match those of the data, and adding random noise at appropriate level, in order to generate the same signal to noise in the observations. The remaining spectra within each order were defined by replicating this reference spectrum. The tests were performed by numerically shifting each spectrum by a prescribed shift relative to the reference one.

As in the case of the spectra reconstructed from real data, three types of

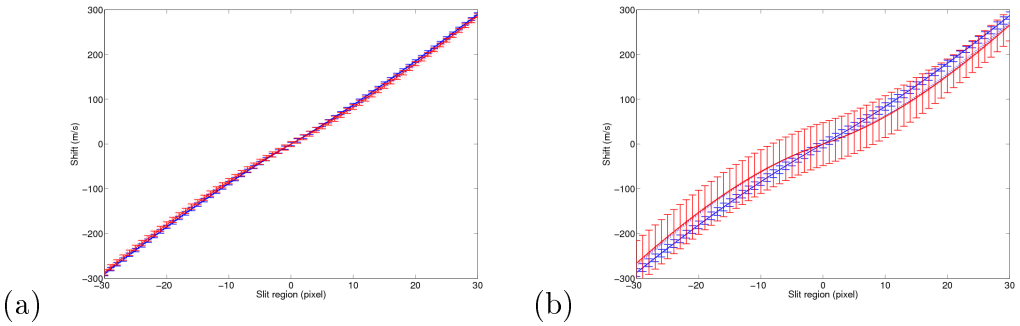

(a) (b)

Figure 2.5: Sensitivity to the signal-to-noise ratio. The plots show the velocity curves relative to the central spectrum, with prescribed shifts between -300 m/s and +300 m/s. The red and blue curves are from the MIT and EEV detector, respectively. (a) Order reconstructed from a spectrum from the order center, SNR = 54; (b) Spectrum with SNR = 12. Both spectra are from one of the exposures from offset 1, case PL.

fully synthetic spectra were generated:

- one with a null relative shift,
- one with a 100 m/s shift between all the spectra in each order and the central spectrum,
- and a third one with a relative shift of 10 m/s between consecutive spectra, ranging from -300 m/s to 300 m/s.

The velocity curve for the zero shift fully synthetic spectra was in accordance with the basic null relative velocity imposed in the synthetic spectra. The same for the case of a imposed shift associated with a relative velocity of 100 m/s. The Doppler shift curve for the 10 m/s step shifted spectra in relation of the central spectrum (between -300 m/s and +300 among the complete set of 61 spectra) also showed high coherence between the imposed shifts and the velocity curve generated by the data reduction algorithm (see figure 2.4). In the baseline case, in which the synthetic spectra were similar to "real" observed data, the velocity curves were consistent with the imposed shift (see figure 2.4). The impact of test variables such as the noise level, the line density and the symmetry of the spectral lines was studied by varying each of these factors independently. Decreasing the signal to noise ratio or decreasing the line density both led to velocity curves lower than the prescribed shift, with a higher discrepancy, in velocity, for spectra farther from the reference one. Increasing the noise level by a factor of four leads to a

20 percent reduction in the retrieved Doppler shift, pixel by pixel, in the velocity profiles obtained from the synthetic spectra relative to the baseline case. Changing the line symmetry, by widening each line in its red side (by increasing the full width at half maximum of the gaussian in its high wavelength side from the line center) led to higher velocities, whereas wider lines in the blue side led to velocities lower than the imposed Doppler shift. Line symmetry is an important factor in the visible wavelength range, since it can be affected by differential atmospheric refraction if not totally compensated by the ADC (atmospheric dispersion corrector) prism.

2.1.10 Kinematical wind models

The final velocities, relative to disk center, and corrected for the various effects discussed above, were then modeled using a kinematical model for the circulation in Venus' mesosphere. Line-of-sight Doppler velocities and horizontal zonal and/or meridional wind components are related by a matrix of projection coefficients for the velocity vector in heliocentric and topocentric reference frames. We calculated these coefficients for the zonal, sub-solar to anti-solar (SSAS), and meridional components of the wind, with the help of a geometrical model (Lellouch et al., 1994). Explicit expressions for these calculations can be found in **?** and were also described in Widemann et al. (2007). Because the instrumental aperture covers a significant fraction of Venus' disk, the projection coefficients for each particular wind regime are calculated over a fine grid of points and then averaged over the aperture on Venus (0.6 arcsec). In order to first interpret the main global wind field at cloud top level we tested two different models:

1. A uniform velocity model between -60°and +60°
   $v_z(\lambda) = -v_{eq}$
2. A solid body model, where λ is the planetocentric latitude
   $v_z(\lambda) = -v_{eq} \times \cos(\lambda)$

Then the χ^2 best-fit has been performed between the measured velocities and the two described models. From the weighted average of all velocity measurements $\bar{v}'_i$ for each day, we fit to a one-parameter zonal circulation. At each individual point, a residue function $\bar{v}'_i - v_{mod,i}$ is retrieved. The parameter v_{eq} (the zonal wind equatorial velocity), minimizes the χ^2 best fit so that:

$$\chi^2_{vel} = \frac{1}{N_{df}} \sum_i \frac{(\bar{v}'_i - v_{mod,i})^2}{\bar{\sigma}'^2_i} \tag{2.8}$$

Where N_{df} is the number of degrees of freedom, $\bar{v}'_i$ is the day-averaged line-of-sight velocity at point i, and $v_{mod,i}$ is the line-of-sight model wind at point i. The fit quality is determined using the reduced χ^2, or $S_{min} = \sqrt{\chi^2_{vel}}$.

Zonal wind

To estimate the zonal wind, we used a 1-wind pure zonal model, as in Machado et al. (2014)). From the weighted average of all the velocity measurements (where the ponderation coefficients used were the inverse of each point variance), obtained on each observations night, we obtain the mean zonal velocity $\bar{v}_z$ in the planetocentric frame:

$$\bar{v_z} = \frac{\sum[c_{z,i} \cdot v'_{k,i}]/[\sigma^2_{k,i}]}{\sum[c^2_{z,i}/\sigma^2_{k,i}]} \tag{2.9}$$

where $c_{z,i}$ is the projection coefficient for point i, $v'_{k,i}$ is the measure k of velocity on the line of sight at point i and $\sigma_{k,i}$ its associated standard deviation. Both uniform velocity and a solid body zonal wind models, yielded similar results in terms of v_{eq}, i.e. we could not distinguish the latitude dependence of the zonal flow between -50°and +50°.

Meridional wind

To estimate the meridional wind, we used a 1-wind pure meridional model, as in Machado et al. (2014)). The subsolar meridian was close to regions of maximum redshift while maximum blueshift was near sub-Earth. At half-phase angle (HPA) the two effects cancel out for the zonal component of the wind field (since the zonal wind is parallel to equator). Along all point lying along the meridian at $[\phi - \phi_E] = 36°$, we therefore assumed that the retrieved Doppler velocities, at those points, cannot be attributed to a zonal component. Hence, the contribution from other wind regimes such as a meridional flow was investigated in our analysis. A χ^2 analysis yields a consistent result for the meridional component, with a marginal significance of the zonal component at the 2-σ level (here we used the same protocol as in Machado et al. (2014)). We monitored the positions along the HPA meridian (see figure 4.1) in our CFHT/ESPaDOnS datasets of Apr. 16 till Apr. 19 (points number: 4, 9, 14, 19, 24, 29, 31, 36, 41, 46 and 51), covering the latitudes from 40°S to 60°N by steps of 10°. We applied a best-fit method to pure meridional wind coefficients (c_m) along this meridian:

$$\bar{v_z} = \frac{\sum[c_{m,i} \cdot v'_{k,i}]/[\sigma^2_{k,i}]}{\sum[c^2_{m,i}/\sigma^2_{k,i}]} \tag{2.10}$$

2.1.11 Altitude of measurments

The visible light is reflected and scattered off Venus' cloud tops. The determination of this altitude level originates from early polarization and photometry studies undertaken by Henson and Hovenier (1974). On the other hand, cloud tops 365 nm UV markings were estimated by Kawabata et al. (1980) to probe the same altitude level (Gierasch et al., 1997; Widemann et al., 2007, 2008).

As discussed by Widemann et al. (2007), the Kawabata et al. (1980) model consists of a main cloud, with particle size of 1.05 μm, underlain by and partly mixed with a haze with $\simeq 0.2$ μm particle size. The optical depth of the haze is about 0.6 at 40 mbar, and varies roughly as $\lambda^{-1.7}$, meaning a $\tau = 1$ level is reached within one scale height of the clouds top at 70 km of altitude (Ignatiev, 2009), see figure **??**. This is also the altitude of the UV cloud markers that enables the cloud tracking wind's measurements technique (Moissl et al., 2009). This coincidence permits to compare magnitudes and variability between ESPaDOnS/CFHT (Machado et al., 2012) results and the ones from tracking of UV markings methods as is the case for VEx/VIRTIS-M, Pioneer/OCPP (*Orbiter Cloud Photopolarimeter*) and Galileo/SSI (*Solid State Imager*).

2.2 Cloud Tracking

Venus Express had the capability of could tracking different depths of the cloud deck, depending on the wavelenght measured.

- UV (300-400 nm): dayside, from sunlight reflectivity (∼65-70 km)
- NIR (∼950nm)(∼950nm): dayside, from sunlight reflectivity (∼61-65 km)
- IR (1.74 and 3.2 μm): nightside, thermal emission (∼45-50 km)
- IR (3.8-5.1 μm): nightside, thermal emission (∼65 km)

The results presented in this work were retrieved by VEx/VIRTIS-M, UV-visible channel at 380nm (center wavelength).

Regarding that the cloud features seen in UV are due to markers in the top cloud layer (approximately the same altitude surveyed by ESPaDOnS/CFHT) the cloud tracking techniques enabled by those cloud contrast (Moissl et al., 2009; Sánchez-Lavega et al., 2008) will produce wind velocity fields that can be compared with the ones obtained with Doppler velocimetry methods that rely in the observations made with ESPaDOnS/CFHT. Also, this coincidence permits to compare magnitudes and variability between ESPaDOnS/CFHT, UVES/VLT (Machado et al., 2012, 2014) results and the ones from cloud tracking of UV markings as is the case for VEx/VIRTIS-M, Pioneer Venus/OCPP and Galileo/SSI. The Visible and InfraRed Thermal Imaging Spectrometer (VIRTIS) is a two-channel imaging spectrometer that operates in the visible range (0.3 to 1 μm) and in the near infrared (1 to 5 μm) (Drossart et al., 2007). In this work we took advantage of VIRTIS-M visible channel, that senses the solar radiation ultraviolet wavelengths, of about 380 nm, back-scattered at cloud tops probing the heights of $66 - 73$ km Venus' dayside. Due to the the highly elliptical polar orbit of Venus Express with apocenter located at south pole side, allied with the long integration time needed to obtain an entire VIRTIS data cube, the privileged region where VIRTIS-M operated, in order to obtain images suitable for retrieve cloud tracked wind measurements, was Venus' southern hemisphere. The achieved spatial resolution on the analysed images strongly varies between 15 km per pixel for high latitudes and about 45 km per pixel for low latitudes.

Venus Express cloud top wind indirect measurements based on tracking using images taken with the VIRTIS instrument (Sánchez-Lavega et al., 2008) indicate nearly constant zonal winds in the Southern hemisphere between 0 and 55 °S, with westward zonal velocities of 105 m/s at cloud tops near

70 km, with detection of a meridional, poleward component with a peak velocity of 10 ± 10 m/s. Short term variability of the zonal flow, which is significant over an hour timescale, at all solar-fixed longitudes and in both hemispheres, is well characterized with the Doppler technique, highlighting the complementarity of the two techniques.

2.2.1 Cloud tracking method

The pairs of VIRTIS-M images selected to make the cloud-tracking were selected in order to maximize both the time interval and the overlapping area among them, so that we optimize the velocity accuracy and the number of vectors, respectively. As a result, the pairs were separated by 80 minutes for the orbit 2918 and shorter times for the case of 2923. The original VIRTIS-M images were navigated and processed to improve the S/N ratio in the same way as described by Machado et al. (2014). Depending on the latitudinal coverage, the couple of images were cylindrically or polar projected with an angular resolution compatible with the image of worst spatial resolution of the pair. We measured the wind speed using visual cloud tracking, as in previous works (Machado et al., 2014).

Chapter 3

Telescope and Instrument

In this section we present a brief description and overview of the ground telescope CFHT and its instrument ESPaDOnS. Details about the space telescope and instrument VEx/VIRTIS-M may be found in section 1.4.2 (Venus Express mission overview) and section 2.2 (Could-tracking method explanation)

3.1 Telescope - CFHT

Canada France Hawaii Telescope - CFHT

The Canada France Hawaii Telescope (CFHT) is located in atop the summit of Mauna Kea (as part of the Mauna Kea Observatory), in the island of Hawaii, at 4200 meters altitude. This 3.6 meter optical/infrared telescope, that became operational in 1979, is a joint facility of the *"National Research Council of Canada"* (NRC), the *"Centre National de la Recherche Scientifique"* of France (CNRS) and the *University of Hawaii* (UH).

3.2 Intrument - *ESPaDOnS*

3.2.1 Instrument description

The **E**chelle **S**pectro **P**ol**a**rimetric **D**evice for the **O**bservatio**n** of **S**tars (ESPaDOnS), at CFHT, is a bench-mounted high-resolution echelle spectrograph and spectropolarimeter which was designed to obtain a complete optical spectrum (from 370 to 1 050 nm) in a single exposure.

ESPaDOns consists of two distinct units, each located at a different place with respect to the telescope:

Figure 3.1: CFH Telescope in Mauna Kea Observatory, Hawaii, U.S.A.

- Cassegrain unit - mounted at Cassegrain focus, includes the calibration/guiding module as well as the polarimeter module;
- Spectroscopic unit - installed in a thermally stable room right at the heart of the telescope building (the *Coudé* room), includes the spectrograph module (the core item of ESPaDOnS in terms of cost and weight) fed from the Cassegrain unit by the fibre link and image slicer module.

The calibration/guiding module includes three components: an atmospheric dispersion corrector (ADC), made of two separate prisms rotating independently from each other, cancelling out the atmospheric refraction in real time; a compact (1k × 1k) ccd camera looking at the instrument aperture (that can be used to autoguide on the star of interest or on any other star present in the 100" camera field of view); and a calibration wheel that can replace the stellar beam by various sorts of calibration light (such as a tungsten lamp for flat fielding purposes, a Thorium-Argon (Th-Ar) lamp used as a wavelength reference, and fully polarised light to impose known vibration directions as a polarising reference).

The spectrograph apparatus consists of a dual pupil configuration with 190 mm, a double set of high-reflectance collimators, a monolithic grating echelle (R2 type) as the diffraction device, with a size of 200 × 400 mm and 79 g/mm, a fully dioptric f/2 camera with 388 mm focal length; also in the instrument optical path there is a high dispersion prism cross-disperser and the detector's CCD (2k × 4.5k) with a pixel size of 0.0135 mm, inside a

cryogenic cooling recipient (dewar cooling system). The optical path is the following: the beam bounces from the main collimator to a flat mirror, and then to a transfer collimator, to the double prism cross-disperser, through the fully dioptric camera and, finally, entering the CCD dewar camera, as seen in the diagram of figure 3.2.

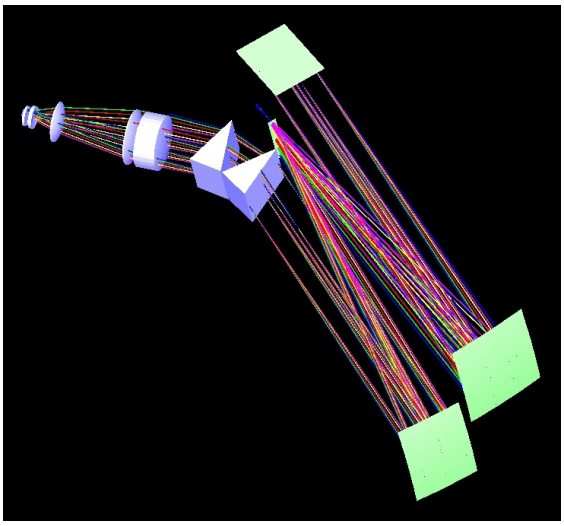

Figure 3.2: ESPaDOnS optical path. (Image from ESPaDOnS website).

The full spectral coverage of the optical domain extends from order number 61, centered at the wavelength of 372 nm, till order 22, centered at 1029 nm, with a spectral resolution of the order of 80 000 (object only mode). The peak throughput of the spectrograph (with ccd detector) is about 40% to 45%, bringing the total instrument peak efficiency at a level of about 15% to 20%.

3.2.2 Modes

The instrument has three different configurations choices:

- **Spectropolarimetric mode** - The two orthogonal states of a given polarization (either circular or linear) are recorded throughout the whole spectral range simultaneously on the ccd detector with the two sets of orders interleaved. The two fibre images are sliced in 3 at spectrograph entrance, yielding an average spectral resolution of about 68 000;

- **First spectroscopic mode ('object+sky')** - The spectra of the target and of the background sky are recorded simultaneously on the ccd

detector (with orders interleaved), the two fibre images are sliced in 3 at spectrograph entrance, yielding an average spectral resolution of about 68 000;

- **Second spectroscopic mode ('object only')** - In this mode (the one used in this work), only the spectrum from the target is collect, the spectrum from the background sky is neglected (for objects bright enough to outshine the sky background, as is the case of Venus in our observations). The single fibre image is sliced in 6 at spectrograph entrance, bringing the average spectral resolution to about 81 000.

3.2.3 Wavelength calibration

An exposure from a Thorium-Argon (Th-Ar) lamp, which spectrum is well known, is used in order to perform the wavelength calibration. Figure 3.3 shows the echellogramme obtained from a Th-Ar lamp calibration exposure.There is an average of about 50 Th-Ar spectral lines per order (about 2000 in total), which are identified by the reduction routine, using reference lists of Thorium and Argon line wavelengths. This will allow to perform an accurate correspondence between the pixel number along, and across, each spectral order and its respective wavelength. From these "anchor points" are produced interpolation polynomials covering the full spectral range. The typical accuracy of this wavelength calibration process is found to be of the order of 0.06 pixels at each given wavelength.

The performed wavelength calibration procedures produce a dispersion law function that is limited by the instrument's spectral resolution. The spectral resolution achieved is derived from the width of the spectral lines obtained at the *echellogramme*. A close up of the individual thorium lines is presented at the figure 3.3 insert (top right), the instrumental average width of individual spectral lines is slightly lower then 2 pixels. The full width at half maximum (FWHM) of individual lines, from the wavelength calibration spectra, is essentially due to a broadening reflecting instrumental causes. From these measurements one can determine the ESPaDOnS spectral resolution (in each mode of operation).

The spectral stability of the measures was assessed by taking repeated calibration frames along a night of observations. After correlating all the image set with the first one taken on the series, it was possible to measure the spectral drifts due to temperature and pressure fluctuations. These results are very handy in order to estimate spurious radial velocities contributions induced from these thermal and mechanical relaxation causes. The average influences in the retrieved radial velocities, from temperature and pressure

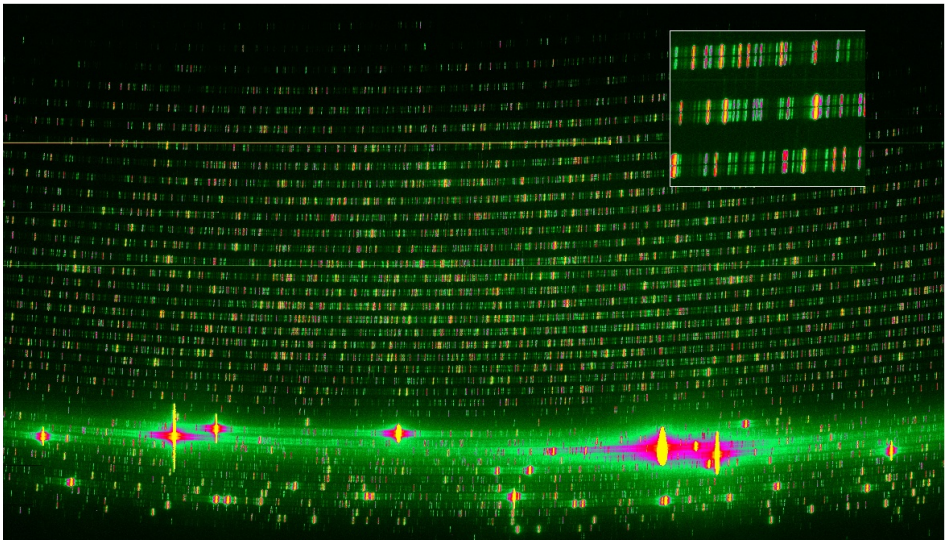

Figure 3.3: ESPaDOnS wavelength calibration with a Thorium Argon (Th-Ar) lamp exposure. In the figure we can see the respective echellogramme. (Image from ESPaDOnS website).

variability, are respectively: -3.5kms^{-1}/°K and 0.3 kms^{-1}/mbar. The estimated relative stability of the instrument is better then 10 m/s rms (Donati, 1997).

Chapter 4

Observations

4.1 CFHT/ESPaDOnS observations

4.1.1 Geometry

The observations were made in 16, 17, 18 and 19 April 2014, using the ESPaDOnS in CFHT. In addition to coordinating with Venus Express, the choice of observing dates offered the best compromise between the need to (i) maximize the angular diameter of Venus and spatial resolution on the disk, and (ii) minimize Venus phase angle and illuminated fraction as we only observe the day side.

Between the 16^{th} and 19^{th} april, Venus was observed at a phase angle Φ (Sun-Target-Observer) of 77.1°-75.6°, with surface brightness at 1.35-1.33 (mag/arcsec), apparent magnitude from -4,27 to -4.22, illuminated fraction between 61.2%-63.2% and an angular diameter of 19.11-18.61 arcsec (see table 4.1 for more details).

The observing strategy has been to displace the entrance fibre of the spectrograph along points on the dayside hemisphere, while taking a reference point exposure between each sequence (reference point at the intersection of Equator and the null zonal Doppler meridian, as in figure 4.1). Exposure times were adjusted at t = 3 sec to obtain a S/N of 400-600 on the continuum and avoid saturation. The sequence of observation points (ajusting the fibre of ESPaDOnS to each positions as is figure 4.1) is displayed in table 4.2.

In our observations with CFHT/ESPaDOnS, back-scattered solar radiation's optical depth, in the visible range, reaches the unity ($\tau = 1$) within one scale height of the cloud tops at 70 km altitude. As discussed in Machado et al. (2014), the first determination of this altitude level comes from Henson and Hovenier (1974) studies of photometry and polarization studies. Ignatiev

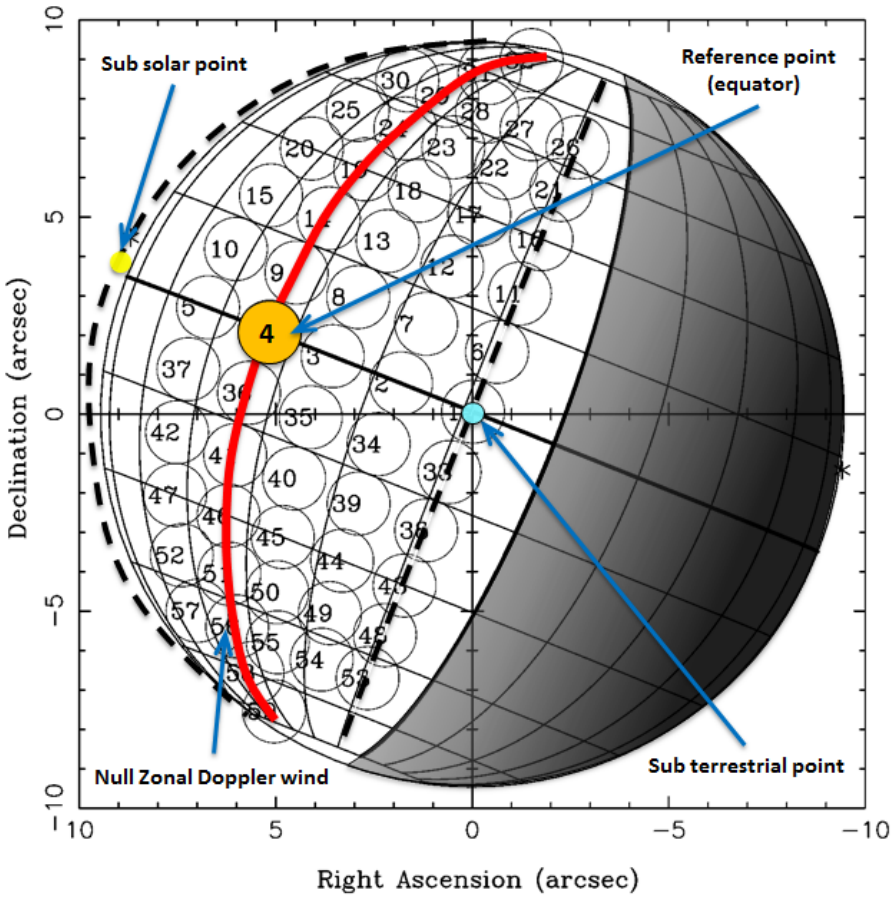

Figure 4.1: Aspect and angular size of Venus as seen from Earth on Apr. 18, 2014, 19h UTC. RA and DEC axis are in arcsec. Celestial North is up. From left to right : (1) thick dashed line is the sub-solar meridian (with the Sun symbol at sub-solar point in yellow) ; (2) red solid line in the half-phase angle (HPA) meridian at $[\phi - \phi_E] = \Phi/2 = 38.2°$; (3) thick dashed-dotted line is the sub-terrestrial meridian (with sub-Earth point as a blue circle) ; (4) local morning terminator is noted as a thick solid grid line east of central meridian. Point numbers as cited in the text are indicated. Planetocentric latitude of sub-Earth and sub-solar points are -0.32° and 1.32°, respectively. The figure illustrates our observing strategy to match CFHT/ESPaDOnS operations (thin black circles) with the respective field of view (1.6"). The point 4 is the reference point (at 0°latitude and 36°longitude) used for the spectral calibration.

(1) Date	(2) UT	(3) Phase angle Φ (°)	(4) Ill. fraction (%)	(5) Ang. diam. (")	(6) Ob-lon/lat (°)	(7) Airmass	(8) seeing (")	(9) Pt size (km)
16 Apr	19:00-21:16	77.1	61.2	19.11-19.10	170.7/ -0,43	1.14-1.25	0.9-0.8	507
17 Apr	16:53-20:47	76.7-76.6	61.5	18.96-18.93	173.1/ -0.38	1.50-1.18	1.0	511
18 Apr	17:10-20:58	76.2-76.1	62.0	18.79-18.77	175.7/ -0.32	1.41-1.20	1.1-0.6	516
19 Apr	17:13-20:34	75.7-75.6	62.4	18.63-18.61	178.3/ -0.27	1.39-1.15	1.1-0.6	520

Table 4.1: Orbital geometry and circumstances of ground-based observations : (1-2) Date/UT interval ; (3-5) disk aspect ; (6) sub-observer longitude and latitude (planetocentric) ; (7-9) observing conditions and geometry.

(2009) stated that the optical depth of the cloud haze is nearly 0.6 at 40 mbar, and varies as $\lambda^{-1.7}$, implying that a $\tau = 1$ level is reached within one scale height of the clouds top roughly at 70 km of altitude, which supports that our ESPaDOnS measurements come essentially from cloud top level. For a detailed discussion please refer to Gierasch et al. (1997); Ignatiev (2009); Widemann et al. (2007, 2008); Machado et al. (2014).

4.1.2 Data reduction

The initial data was reduced and retrieved by a pipeline software named "Libre-ESpRIT", which is available to use in any observational run with the ESPaDOnS. This pipeline produces one file for each point observation in the format *".out"*, which is a text format. The first step in our work was to export (manually) the data we needed from each pointing, from each file *.out* to an excel page. Then, we analyzed manually which points suffered an anomaly (such as a telescope drift or passing clouds) and which data may have been compromised. The next step was to run our manually reduced data through *IDL* programs, introducing the theoretical models and calculating the mean wind values (zonal and meridional). Some of this *IDL* programs were computed by myself, although the major complex programs were already developed and tested by Dr. Pedro Mota Machado, Dr. David Luz and Dr. Thomas Widemann. Although the *IDL* programs were used to compile the data, the plots were produced using the program *Grapher*.

Most of my personal contribution for this work was in the data reduction process (exporting data manually to excell sheets), the IDL programming to compile the data (creating and using IDL programs), and the production of

(1) Seq. nb	(2) Loc.	(3) Time span (UT)	(4) Points order
Apr. 16			
[1]	Equ.	19:01-19:33	4-4-5-4-3-2-1-4
[2]	N lat 10°	19:35-19:58	4-10-10-9-8-7-6-6-4
[3]	N lat 20°	19h59-20:25	4-15-14-13-12-12-11-4
[4]	N lat 30°	20:26-20:41	4-20-19-18-17-16-4
[5]	N lat 40°	20:42-21:03	4-25-24-23-22-21-4
Apr. 17			
[6]	Equ.	16:53-17:35	[4]-4-4-5-(4)-[3]-[2]-[1]-4
[7]	N lat 10°	17:36-17:55	[4]-10-(10)-9-[8]-[7]-[6]-[4]
[8]	N lat 20°	18:00-18:24	4-[15]-14-[13]-4
[9]	N lat 30°	18:26-18:43	4-20-19-[18]-[17]-4
[10]	N lat 40°	18:50-19:21	4-[25]-24-(24)-23-[22]-[21]-4
[11]	S lat 10° - 30°	19:22-20:25	(4)-4-(37)-37-36-47-46-45-44-(43)-[4]-4
Apr. 18			
[12]	$[\phi - \phi_E] = 36°$, N	17:10-17:30	4-9-14-19-24-29-31-32-4
[13]	$[\phi - \phi_E] = 36°$, S	17:31-17:55	4-36-41-(46)-46-46-[51]-56-[58]-58-4
[14]	$[\phi - \phi_E] = 0°$	17:58-18:37	[4]-[1]-[6]-[11]-[16]-[21]-[4]-[33]-[38]-[43]-[48]-[53]-[4]
[15]	$[\phi - \phi_E] = 24°$	19:57-20:58	4-3-8-13-18-[4]-23-28-4-3-4
Apr. 19			
[16]	N lat 20°	17:13-17:29	4-15-14-13-12-11-4
[17]	N lat 30°	17:31-17:45	4-20-19-18-17-16-4
[18]	N lat 40°	17:46-18:10	4-(25)-[25]-25-24-[23]-23-22-21-21-4
[19]	S lat 20°	18:11-18:25	4-42-41-40-39-38-4
[20]	S lat 30°	18:27-18:47	4-47-46-46-45-44-43-43-4
[21]	S lat 40°	18:48-19:11	4-52-51-51-50-49-48-4
[22]	N lat 20°	19:12-19:26	4-15-14-13-12-11-4
[23]	N lat 30°	19:27-19:47	4-20-19-18-17-16-16-4
[24]	N lat 40°	19:49-20:06	4-25-24-23-22-21-4
[25]	S lat 20°	20:16-20:34	4-42-41-41

Table 4.2: Scanning sequences on Venus' dayside hemisphere using CFHT/ESPaDOnS during the Apr. 16-19, 2014 observing run : (1) sequence number; (2) location on disk; (3) UT time interval; (4) points acquisition order; points in parenthesis have been observed but not included in the kinematical best fits either for their lower S/N and/or limb or high SZA geometry; (5) exposure repetition: each point is acquired 3 times to check for internal consistency. Points in brackets were discarded from analysis due to severe drift, seeing or tracking issues.

all the plots used to present the results (made with *Grapher*).

4.2 VEx/VIRTIS-M observations

Obtaining coherent results when measuring the winds of Venus with different techniques (Doppler and cloud-tracking) is essential towards a mutual validation of both methods. To this aim, our ground-based Doppler measurements were carried out in coordination with observations by ESA's Venus Express mission, and they extended during three orbits (from 2918 to 2921). Since Venus Express had a polar orbit, some of the instruments onboard the spacecraft demanded long exposure times and they were, thus, unable to carry out observations close to the pericenter. For this reason, ground-based observations were chosen to be coincident with VEx apocentric observations of the south hemisphere of Venus.

Several sets of ultraviolet images - able to sense the cloud tops through the scattered/absorbed radiation at about 70 km (Ignatiev, 2009) - were acquired with the Visible and InfraRed Thermal Imaging Spectrometer (VIRTIS-M) (Drossart et al., 2007) and the Venus Monitoring Camera (VMC) (Markiewicz et al., 2007). Wavelengths of 380 and 365 nm were chosen for VIRTIS-M and VMC, respectively. As VMC required shorter exposure times, it also acquired short-time sets of high spatial resolution images (typically less than 10 minutes in each orbit) closer to VEx pericenter (thus not strictly simultaneous with ESPaDoNS) and covering the northern hemisphere of Venus. Unfortunately, the S/N of VMC apocentric observations during these orbits was low and not trustable for cloud-tracking, while the high velocity of VEx during these pericentric observations didn't allow enough spatial overlap to track cloud features between pairs of images. In the case of the VIRTIS-M, apocentric observations were made only during orbits 2918 and 2923, with the first being the only one coincident with our observations. Although two days after our ground-based observation, the images from the orbit 2923 were also analyzed since they were the closest in time and permitted to have a control about the wind variability with time.

The detailed information about the VIRTIS-M images used in this work can be found in Table 4.3, and a comparison of the spatial coverage for VIRTIS-M and ESPaDoNS can be seen in Figure 4.2. In addition to clear temporal changes in the cloud morphology as seen from VIRTIS-M images, we also checked from VIRTIS-M and VMC observations that there was an intense wave activity apparent on the albedo of the cloud tops during the all days of ESPaDoNS observations (see Figure 4.3), with wavelengths ranging from tens (Fig. 4.3a-c) to hundreds of km (Fig. 4.3d) which are consistent with gravity waves (Peralta et al., 2014).

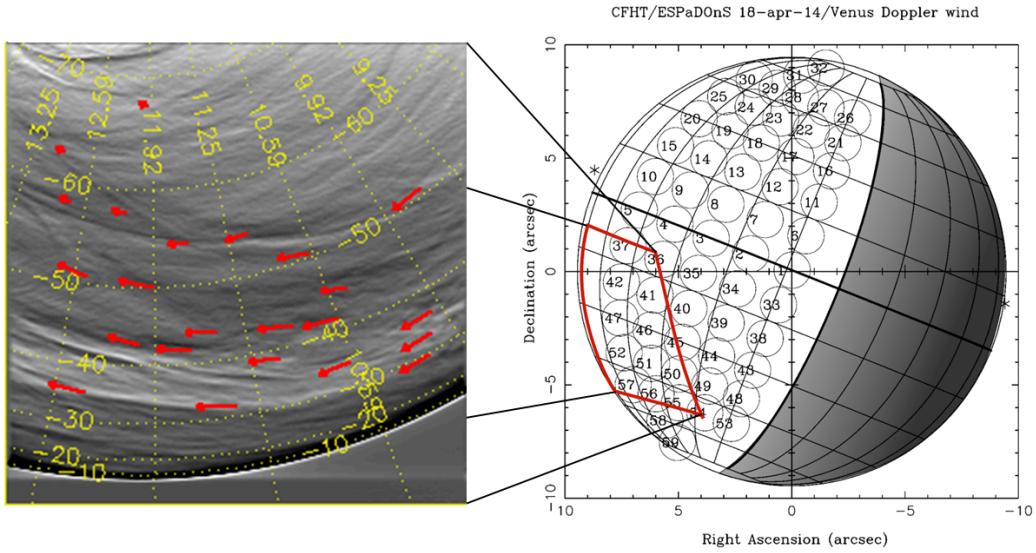

Figure 4.2: Right side: aspect of Venus disk as seen from Earth (as in figure 4.1) with superimposed Venus-Express VIRTIS instrument's FOV. The figure illustrates our observing strategy to match CFHT/ESPaDOnS operations (thin black circles) and ESA/Venus Express VIRTIS-M instrument FOV (red distorted rectangle) during orbit 2923. Left side: zoom-out of an image (VV2923_08) obtained with VIRTIS-M at 21 Apr. 2014 (orbit 2923), the latitudes covered the range from 10°S to 50°S and the local time spans from 10h till 13h. On the zoomed image (VV2923_08) we can see tracers (red arrows) marked on cloud features that will correspond to matching cloud features on this image's pair (VV2923_11) obtained 48 minutes later.

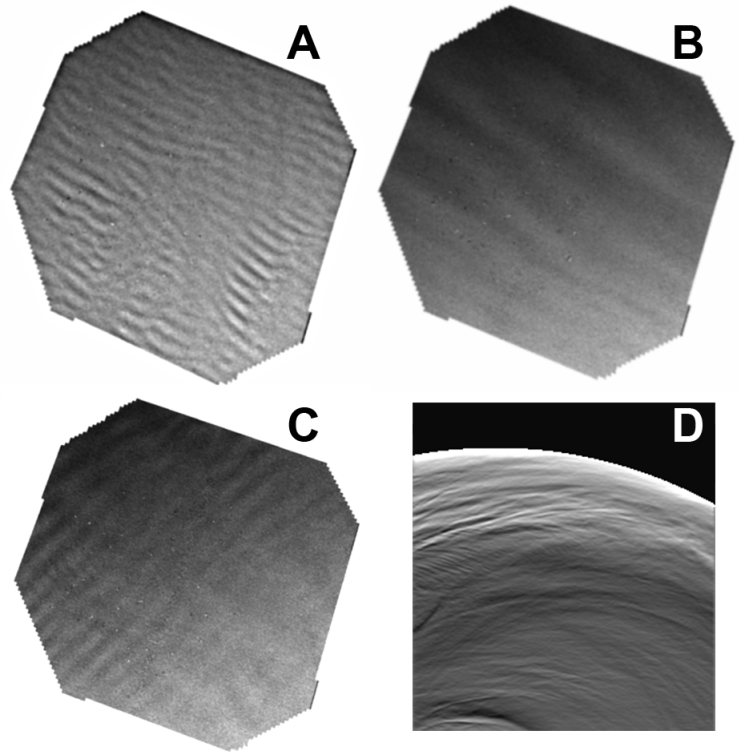

Figure 4.3: Examples of recurrent presence of gravity waves on the dayside cloud tops during our observations: (A) waves at 70°N and 10:31 LT in a VMC image with spatial resolution of 147 m and taken on 17 of April 2014, (B) waves at 73°N and 10:37 LT in VMC image with resolution 135 m during 18 April 2014, (C) waves at 77°N and 10:43 LT in VMC image with resolution of 132 m during 19 April 2014, and (D) waves at 45°S and 12:30 LT in VIRTIS-M image with resolution of 19 km during 21 April 2014.

(1) VEx orbit	(2) Qubes pairs	(3) Date (yyyy/mm/dd)	(4) Time interval (min)	(5) Latitude range	(6) Local time range	(7) Number of points
2918	VV2918_04 VV2918_09	2014/04/16	80	50°S-90°S	10h−14h	08
2918	VV2918_06 VV2918_11	2014/04/16	80	20°S-50°S	12h−15h	11
2918	VV2918_07 VV2918_12	2014/04/16	80	20°S-70°S	09h−12h	14
2918	VV2918_13 VV2918_16	2014/04/16	80	10°S-40°S	11h−13h	10
2923	VV2923_00 VV2923_03	2014/04/21	60	40°S-90°S	09h−14h	13
2923	VV2923_04 VV2923_07	2014/04/21	60	20°S-70°S	09h−13h	23
2923	VV2923_08 VV2923_11	2014/04/21	48	10°S-50°S	10h−13h	25

Table 4.3: ESA Venus Express/VIRTIS-M UV-visible channel at 380 nm observations circumstances : (1) orbit number ; (2) VEx-VIRTIS hyperspectral images or "Qubes" pairs as defined by Cardesín (2010) ; (3) UT date ; (4) time interval between selected image pairs ; (5-6) corresponding latitude and local time range. The imaging spatial resolution varies between 15 km per pixel for polar latitudes and about 45 km per pixel for equatorial ones ; (7) number of cloud tracers identified in image pairs. The observations from 16 Apr., 2014, are coordinated with ESPaDOnS' ones, which allows us to directly compare winds measurements from same time, same location, upon Venus. The VIRTIS-M observations from 21 Apr. will permit us to better address temporal variability of the Venus' winds, regarding that this observing date increases, considerably the time span of our investigation in this run.

Chapter 5

Results

5.1 CFHT/ESPaDOnS results

5.1.1 Mean zonal circulation

After applying all the necessary corrections (Young effect and spectral drift), and weighed averaged all the measures of each position for each day, we applied the respective theoretical models, under the assumption of a pure zonal one-wind system, to all data points with latitudes between -50°and +50°(as the model predicts), to estimate the mean zonal wind (parallel to equator).

The results obtained, with the CFHT/ESPaDOnS observations, for the mean zonal and mean meridional winds, with a best-fit reduced χ^2 at 2σ and 3σ confidence, are presented in table 5.1 (results for day-averaged wind velocity $\overline{v}'_i$).

Day-averaged zonal wind

By weigh averaging all the measures for each position, we obtained a single mean value for each position, for all the 4 days. With this data, we produced a color map of the zonal mean velocity for each position, as seen in figure 5.1.

CFHT/ESPaDOnS observations took the form of observing sequences between April 16^{th} and 19^{th}. Sequences [1-5] (Apr. 16) were acquired across the dayside hemisphere at latitudinal bands 10-degrees apart at latitude/local time points of table 4.2 in a 2-hours time scale. On this day of observations ESPaDOnS has a projected field of view of 507 km at Venus' disk center. The upper-left of figure 5.1 locates points acquired on that day with the resulting horizontal wind superimposed to each point.

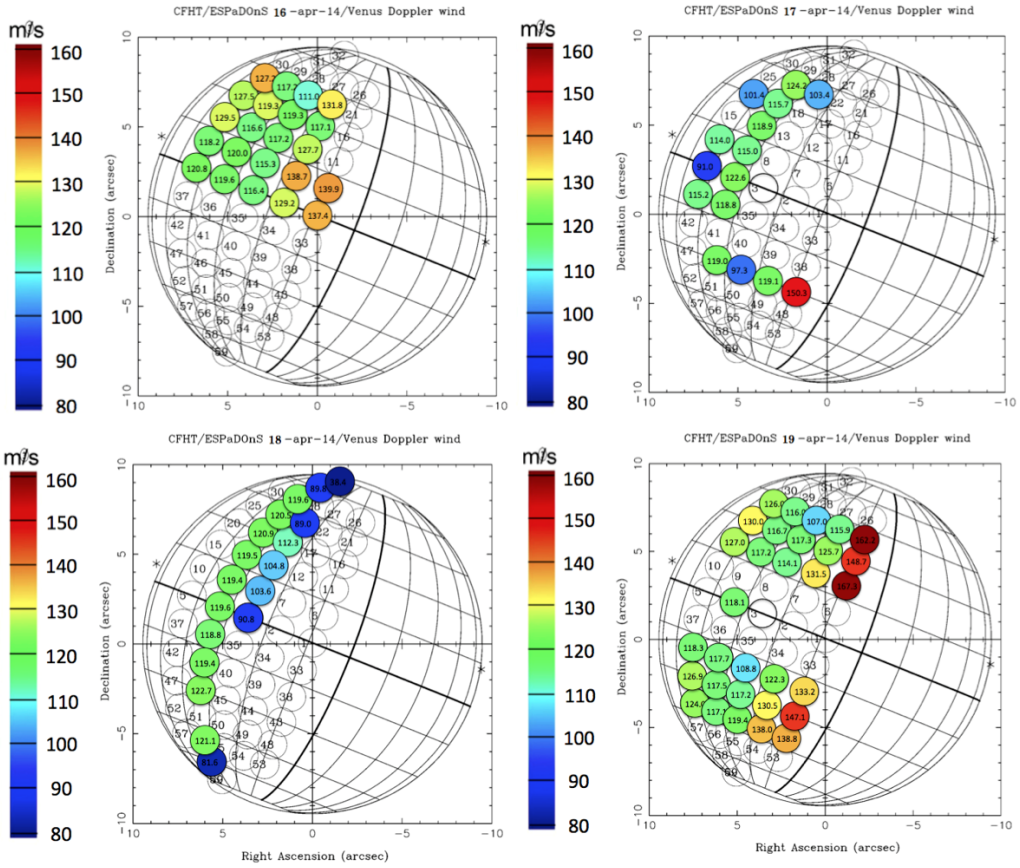

Figure 5.1: Upper left: Results for day average wind velocity $\overline{v}'_i$ for observing sequences [1-5] (Apr. 16) at latitude/local time points of table 4.2. Values are in m/s. On this day of observations ESPaDOnS has a projected field of view of 507 km at Venus' disk center. Upper right: Results for Apr. 17, 2014 (sequences [6-11]). FOV is 511 km at Venus' disk center. Bottom left: The same for Apr. 18, 2014 (sequences [12-15]). FOV is 516 km at Venus' disk center. Bottom right: The same for Apr. 19, 2014, (sequences [16-25]). FOV is 520 km at Venus' disk center.

Date	Mean zonal wind (m s^{-1}) $\overline{v}_z$	reduced χ^2	2σ m s^{-1}	3σ m s^{-1}
16 Apr. 2014	119.6	1.49	± 16.5	±24.8
17 Apr. 2014	122.6	3.38	± 31.3	±62.5
18 Apr. 2014	119.6	2.27	± 26.0	±39.5
19 Apr. 2014	118.1	1.78	± 19.5	±29.5
Date	Meridional velocity (m s^{-1}) $\overline{v}_m$	reduced χ^2	2σ m s^{-1}	3σ m s^{-1}
16-19 Apr. 2014	22.5	1.68	±15.5	±20.3

Table 5.1: CFHT/ESPaDOnS mean zonal and mean meridional flow results. - (a) Mean zonal velocity $\overline{v}_z$ on April 16, 17, 18 and 19, 2014 data. The 1-wind regime fit is applied to the entire probed region $v_{z,i}$ data points. Best-fit reduced χ^2 is indicated at 2σ and 3σ confidence. (b) Mean meridional wind velocity $\overline{v}_m$ fit along HPA meridian ($[\phi - \phi_E] = \Phi/2 \simeq$ -38°), obtained at 2σ and 3σ confidence level.

Observed measurements of Apr. 17 (sequences [6-11]) appear in the upper right part of figure 5.1. Observations on Apr. 17 were frequently interrupted by clouds and this is reflected by the larger confidence interval at 2σ and 3σ appearing in table 5.1 for the mean zonal circulation.

On Apr. 18, 2014 (sequences [12-15] bottom-left part of figure 5.1), our priority was given to repeated observations of the HPA (null-Doppler meridian) in search for the meridional component of the wind (see the following subsection 5.3). The mean-zonal circulation was also retrieved from the available sequences, especially using the 30°S latitude band.

On Apr. 19, 2014 (sequences [16-25]), N and S hemispheres were symetrically explored during a 3:20 period [17:13 UT-20:34 UT] for the monitoring of zonal wind short term variability. This is further described in Section 5.1.3.

The best-fit results for the four days of observations are self-consistent, with $\overline{v}_z$ = (119.6 ± 16.5) ms^{-1} on Apr. 16, $\overline{v}_z$ = (122.6 ± 31.3) ms^{-1} on Apr. 17, $\overline{v}_z$ = (119.6 ± 26.0) ms^{-1} on Apr. 18, and $\overline{v}_z$ = (118.1 ± 19.5) ms^{-1} on Apr. 19, with a best quality of fit on Apr. 16 and Apr. 19 (S_{min} = 1.49 and 1.78, respectively). Although the overall fit looks reasonable, the fit is statistically poor on Apr. 17 and 18 (S_{min} = 3.38 and 2.27, respectively), suggesting that individual error bars may be underestimated, or that the circulation is more complex than described by the model.

Zonal wind latitudinal profile of CFHT/ESPaDOnS $\overline{v}_{z,i}$ velocities ob-

tained from a weighed average on all data present on our observations (Table 5.2), and consolidated by the observations from all days of observations, are shown in Fig. 5.2.

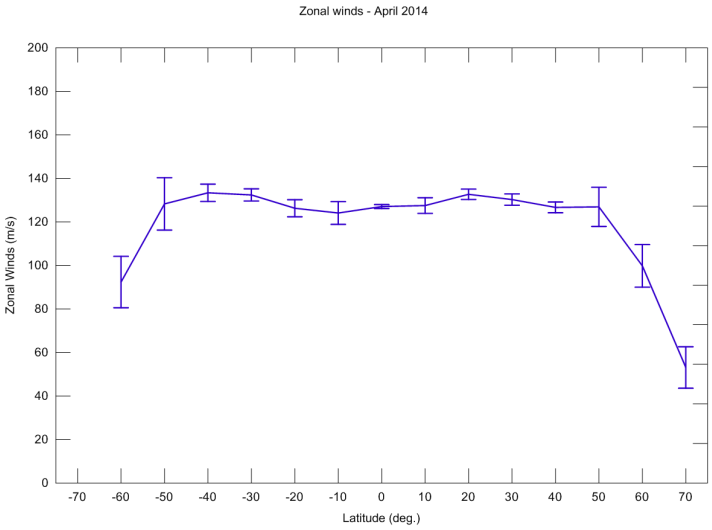

Figure 5.2: Zonal wind latitudinal profile, $\overline{v}_{z,i}$ velocities combine all Apr. 16-19, 2014 CFHT/ESPaDOnS observations of table 5.2). The weighing coefficients reflect the zonally averaged variance of each latitude. We note an almost uniform average zonal wind component ($\overline{v}_{z,i}$) between mid-latitudes, the presence of mid-latitudes jets and a sharp decrease of zonal wind for higher latitudes (higher than 50°).

5.1.2 Meridional wind

New evidence for meridional wind flow

The data gathered in day 18^{th} April allowed us, after applying the respective theoretical model, to estimate the meridian wind flow for the Hadley cell, from -50°to +60°latitude. The points in the Null-Zonal Doppler meridian (longitude = 36°) are points in which the Doppler shift effect cancels out, due to the half-angle phase location, as explained earlier. For those points, we assumed that the Doppler measures were due to meridian wind flow caused by the Hadley cell structure.

A poleward meridional wind component is determined within the 2-σ statistical significance by selecting the line-of-sight measurements on half-phase angle meridian HPA. Table 5.1 shows the mean meridional wind velocity $\overline{v}_m$ fit along HPA meridian ($[\phi - \phi_E] = \Phi/2 \simeq$ -38°), obtained at 2σ and 3σ

confidence level by combining HPA data from Apr. 16-19 sequences [1-25], analyzing the entire data set with a single meridional model.

For the first time, a meridional wind component at cloud top is simultaneously observed from the ground in the two hemispheres (figure 5.3). Negative velocities in the S hemisphere on figure 5.3 reflects poleward cloud top motion, while positive values in the N hemisphere also indicate a poleward motion. This is in agreement with a Hadley cell's upper branch, were the meridional wind flows from equator region to higher latitudes. We note the almost symmetrical behavior of the meridional flow between N and S hemispheres. The dashed line is a fit to a pure meridional model flow with $\overline{v}_m = (22.5 \pm 15.5)$ m s^{-1} (see table 5.1).

Our meridional wind model is assumed to vary sinusoidally with latitude, having zero velocity at equator and the poles, and a maximum value at 45° latitude. It can be noted that our measurements differ significantly from this model poleward of 50°, meaning lower winds than predicted at high latitudes near the cold collar.

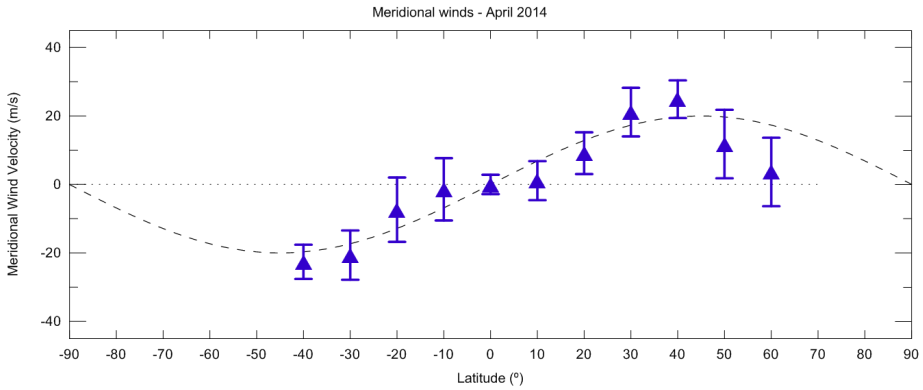

Figure 5.3: Meridional wind component determined within the 2- σ statistical significance by consolidating the line-of-sight measurements along half-phase angle meridian HPA, averaged over Apr. 16-19 sequences. Negative velocities in southern hemisphere means aerosols motion away from equator, as is the case of the positive values of meridional wind in northern hemisphere (remind that our reference is position number 4, at equator). The dashed line is a fit to a pure meridional model flow with $\overline{v}_m = (22.5 \pm 15.5)$ m s^{-1} (see table 5.1). It is assumed to vary sinusoidally with latitude, having zero velocity at equator and the poles, and a maximum value at 45° latitude.

5.1.3 Zonal wind variability (spatial and temporal)

$[\phi - \phi_E]$ longitudinal (local time) variations of zonal wind velocities $\overline{v}_{z,i}$

Here we present the latitudinal profile (fixed latitude) for each day of CFHT/ESPaDOnS zonal wind velocities $\overline{v}_{z,i}$ (days 16, 17, 18, 19 April, 2014). Each presented latitudinal wind velocity results from a weighed average along each latitude band measured on each day of observations. The weighing coefficients were the inverse of the variance associated to each velocity measurement. Figure 5.4 shows a comparison of day-averaged zonal wind $\overline{v}_{z,i}$ at various latitudinal bands on different days of April 2014 observations. On each plot, X-axis is west longitude to sub-terrestrial meridian. $[\phi - \phi_E]$, and the corresponding to local times. Y-axis are $\overline{v}_{z,i}$ determination. Fit results to a pure zonal wind per latitudinal band $\overline{v}_{z,lat}$ are indicated in table 5.2.

Table 5.2 shows 1-wind zonal circulation per latitudinal bands $\overline{v}_{z,lat}$ is fit to day-averaged wind values $v_{z,i}$ of figure 5.4, with their statistical significance at the 2-σ level. The weighing coefficients were the inverse of each retrieved velocity's variance.

Figure 5.5 shows latitude bands of day-averaged horizontal zonal wind $\overline{v}_{z,i}$ as in figure 5.4. Fit results to a pure zonal wind per latitudinal band $\overline{v}_{z,lat}$ are indicated in table 5.2.

Temporal variation - By comparing the same latitudinal band for different days (figure 5.4, we can analyze the time evolution and variability of zonal winds. For 40°N and 30°S latitudinal bands, is notorious a slight variation in zonal wind velocity, in the points located at $[\phi - \phi_E]$ = -12° and $[\phi - \phi_E]$ = -24°, respectively. These variations were measured with two and three day intervals for 40°N and 30°S latitudinal bands, respectively. Although these variations are of the order or 20 m/s, they are of the same order of the respective error bars, thus, they may not represent substantial temporal variation. Additional, the variation in the latitudinal bands 30°S may be due to the difficulties faced during the observations of day 17 Apr (high cirrus clouds passing during observations).

Spatial (latitudinal) variation - By comparing all the latitudinal bands of each day-averaged horizontal zonal wind $\overline{v}_{z,i}$ (figure 5.5), no unambiguous spatial variation can be derived, since all latitudinal bands show similar profiles (variations in the order of the error bars - 10m/s). The observations made in the 17^{th} and 18^{th} April were more focused on the Half-Phase meridian (longitude -36°), thus, no significant analysis could be done for latitudinal and temporal variation from said data. In both figures(5.4 and 5.5) it is noticeable the very similar profiles with velocities decreasing from the

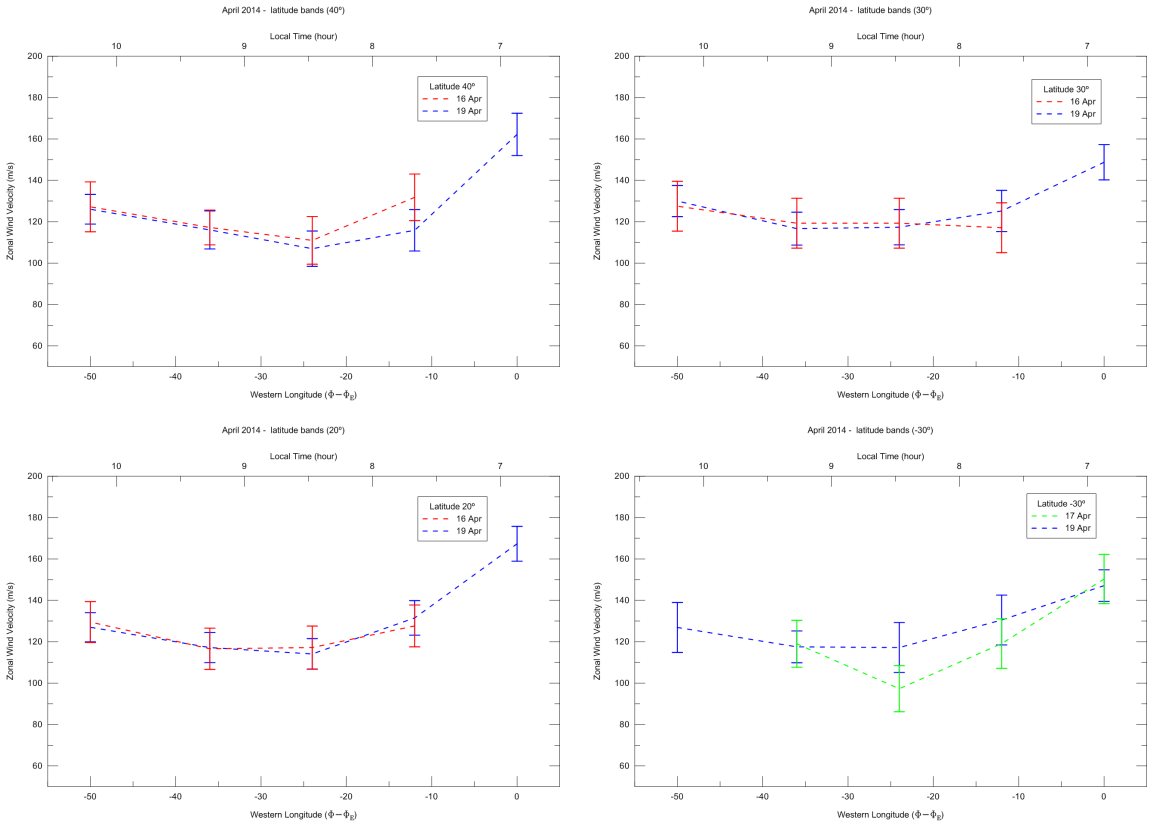

Figure 5.4: Latitude bands of horizontal zonal wind $\overline{v}_{z,i}$ across ESPaDOnS' dayside local-time range between 6:50a and 10:00a. X-axis is west longitude to sub-terrestrial meridian. $[\phi - \phi_E]$, corresponding to local times 6:50a (0°), 7:40a (-12°), 8:30a (-24°), 9:15a (-36°), 10:10a (-50°) from terminator (left) to sub-solar region (right). Y-axis are $\overline{v}_{z,i}$ results. Fit results to a pure zonal wind per latitudinal band $\overline{v}_{z,lat}$ are indicated in table 5.2. Top left: Comparison between day 16 and 19 April, 2014, for 40°N latitude band. Top right: the same but for 30°N. Bottom left: Comparison of 20°N latitude band for day 16 and 19 April, 2014. Bottom right: Comparison of 30°S latitude band for day 17 and 19 April, 2014.

	Dates			
	Apr. 16, 2014	Apr. 17, 2014	Apr. 18, 2014	Apr. 19, 2014
Lat. band	$\overline{v}_{z,lat}$ (m s^{-1})	$\overline{v}_{z,lat}$ (m s^{-1})	$\overline{v}_{z,lat}$ (m s^{-1})	$\overline{v}_{z,lat}$ (m s^{-1})
70°S	-	-	38.4 ± 10.5	-
60°S	-	-	89.8 ± 10.8	-
50°S	-	-	119.6 ± 9.9	-
40°S	121.0 ± 5.2	115.0 ± 6.8	97.8 ± 9.0	123.9 ± 3.9
30°S	120.8 ± 6.0	108.8 ± 8.4	120.1 ± 10.6	127.5 ± 3.7
20°S	122.8 ± 5.0	118.9 ± 11.2	115.3 ± 9.3	129.5 ± 3.4
10°S	123.7 ± 5.1	114.2 ± 10.1	115.4 ± 8.2	-
0°S	120.3 ± 2.0	116.2 ± 6.2	118.6 ± 2.4	118.8 ± 4.8
-10°S	-	-	118.8 ± 16.0	129.6 ± 4.3
-20°S	-	120.5 ± 5.8	119.4 ± 10.3	126.7 ± 4.4
-30°S	-	-	122.7 ± 6.9	-
-40°S	-	-	-	-
-50°S	-	-	121.1 ± 13.2	-
-60°S	-	-	81.6 ± 13.0	-

Table 5.2: 1-wind zonal circulation per latitudinal bands $\overline{v}_{z,lat}$ is fit to day-averaged wind values $v_{z,i}$ of Fig. 6, with their statistical significance at the 2-σ level.

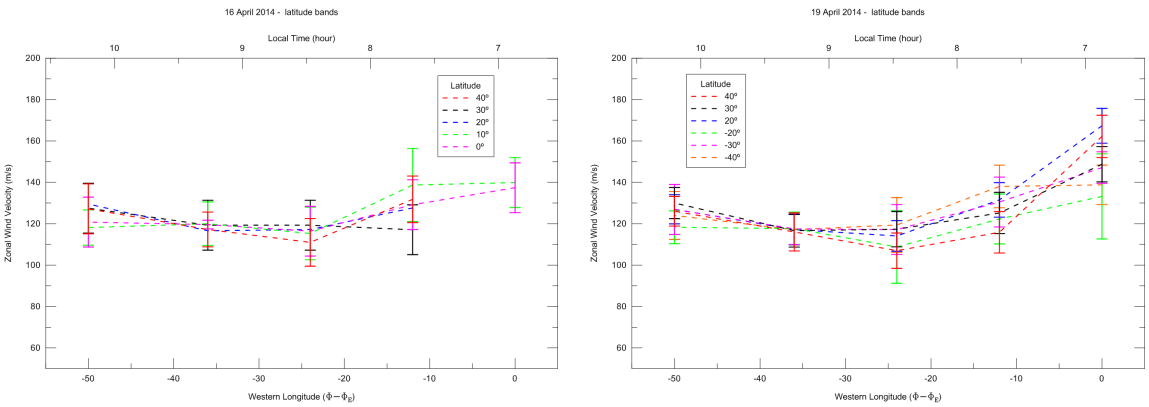

Figure 5.5: Latitude bands of day-averaged horizontal zonal wind $\overline{v}_{z,i}$ as in figure 5.4. Fit results to a pure zonal wind per latitudinal band $\overline{v}_{z,lat}$ are indicated in table 5.2. Left: Latitude bands for day 16 April, 2014. Right: Latitude bands for day 19 April, 2014.

terminator onwards (western longitude direction), with a slight increase at longitude -50°S. The systematic higher wind velocities in the sub-terrestrial meridian ($[\phi - \phi_E] = 0°$) can be interpreted in terms of a thermal solar tide, as stated by Machado et al. (2014) and Sánchez-Lavega et al. (2008).

Latitudinal variations of zonal wind velocities $\overline{v}_{z,i}$

Here we present the longitudinal profile (fixed longitude) for each day of CFHT/ESPaDOnS zonal wind velocities $\overline{v}_{z,i}$ (days 16, 17, 18, 19 April, 2014). Each presented longitudinal wind velocity results from a weighed average along each latitude band measured on each day of observations. The weighing coefficients were the inverse of the variance associated to each velocity measurement.

Comparison from day-averaged longitude bands of zonal wind $\overline{v}_{z,i}$ between observational days, across ESPaDOnS' dayside, are presented in figure 5.6 (X-axis are $\overline{v}_{z,i}$ results and Y-axis is latitudes along Venus). Referred longitudes correspond to west longitude to sub-terrestrial meridian $[\phi - \phi_E]$, where 0° correspond to local time of 6:50a, -12° to 7:40a, -24° to 8:30a, -36° to 9:15a and -50° to 10:10a.

Spatial variability of day-averaged on relative longitudes bands, in solar-fixed coordinates, of zonal wind $\overline{v}_{z,i}$ across ESPaDOnS' dayside, are presented in figure 5.7 (X-axis are $\overline{v}_{z,i}$ results and Y-axis is latitudes along Venus). Referred surveyed longitudes and local times are as in figure 5.6.

Temporal variation - By comparing the same longitudinal band for different days (figure 5.6, we can analyze the time evolution and variability of zonal winds. None of the longitude bands show any unambiguous variation with time, with the exception of longitude -50°(10:10a local hour). However, the wind velocity variations shown in the said longitude band (-50°) may also be due to the adverse observing conditions encountered during the observations of day 17 Apr (high cirrus clouds passing in front of the FOV). The bottom left plot (figure 5.6) shows a highly consistent latitudinal profile along all the 4 days for longitude -36°. This profile clearly shows a steady decrease in wind velocity from 50°latitude (both North and South) towards the poles, as expected from the zonal wind models and in agreement with previous results.

Spatial (longitudinal) variation - By comparing all the longitudinal bands of each day-averaged longitude bands $\overline{v}_{z,i}$ (figure 5.7), the most relevant variation is seen in the bottom right plot (19 Apr.): the 0°profile shows higher wind velocities comparatively to all other longitudinal profiles. As previously stated, this may be explained by a presence of solar tide in the meridians near the terminator. Day 17^{th} Apr. shows, again, some wind velocity variations in the order of 20 m/s.

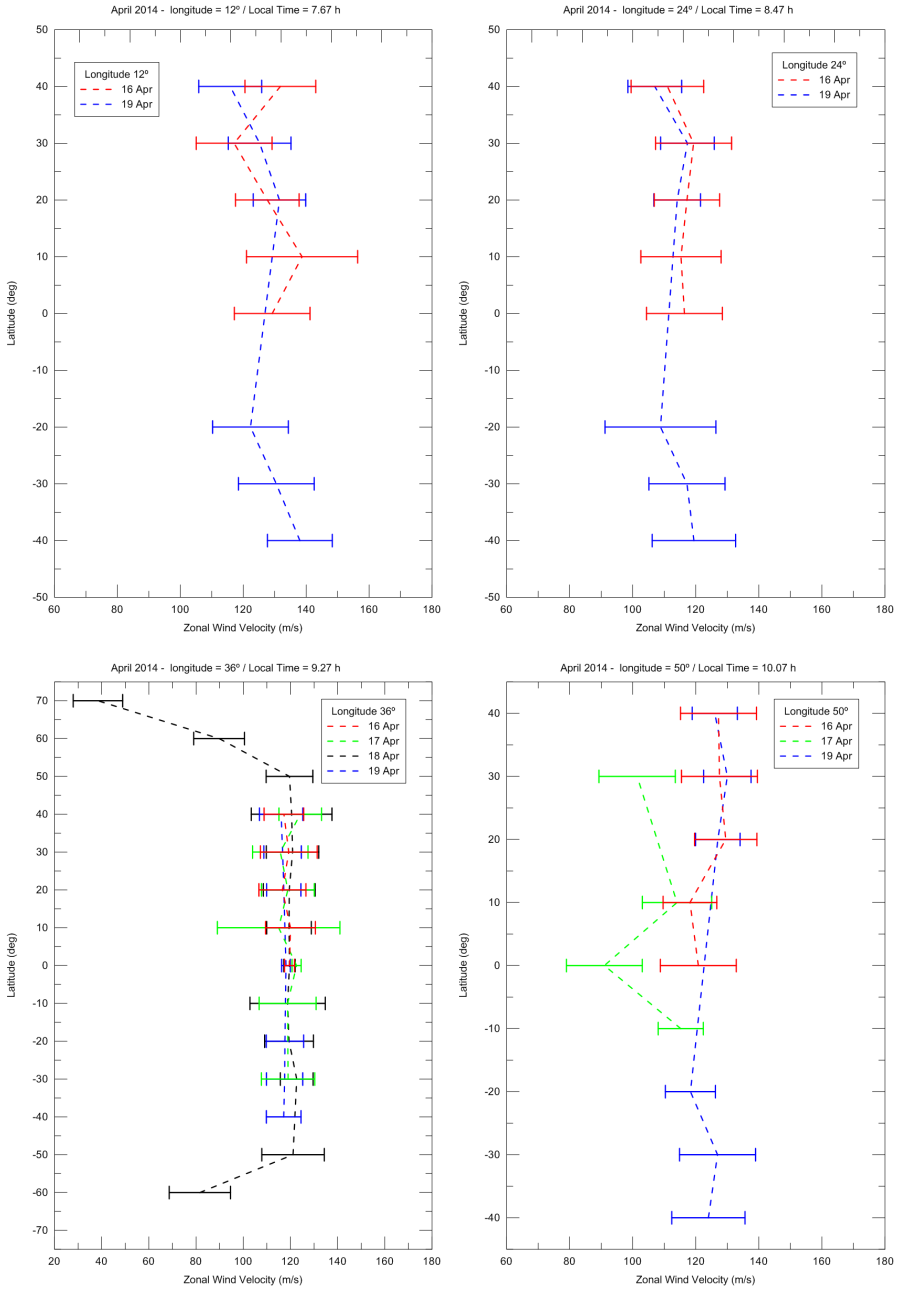

Figure 5.6: Comparison from day-averaged longitude bands of zonal wind $\overline{v}_{z,i}$ between observational days, across ESPaDOnS' dayside. X-axis are $\overline{v}_{z,i}$ results. Y-axis is latitudes along Venus. Top left: temporal variability study, of zonal wind for local time of 7:40a (-12° western longitude from sub-terrestrial point), between day 16 Apr. and 19 Apr., 2014. Top right: temporal variability, as in precedent case, for 8:30a local time (-24°) between day 16 and 19 Apr. Bottom left: temporal variability of 9:15a (36° western longitude from sub-terrestrial meridian, ESPaDOnS' FOV along this meridian includes the HPA meridian) between days: 16, 17, 18 and 19 Apr. Bottom right: same as precedent but for 10:10a local time (-50° longitude) for days 16, 17 and 19 Apr.

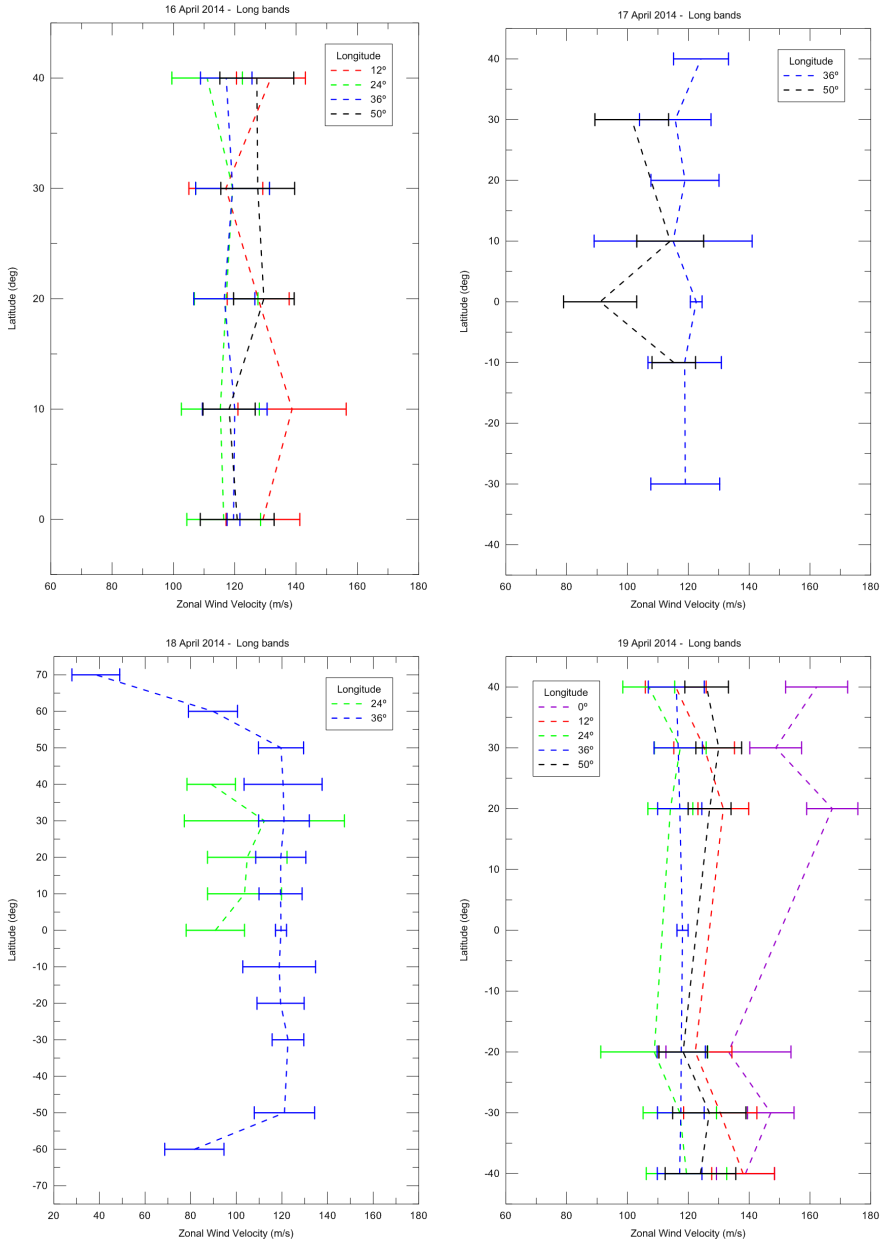

Figure 5.7: Spatial variability study of day-averaged on relative longitudes bands, in solar-fixed coordinates, of zonal wind $\overline{v}_{z,i}$ across ESPaDOnS' day-side. X-axis are $\overline{v}_{z,i}$ results. Y-axis is latitudes along Venus. Referred surveyed longitudes and local times are as in figure 5.6. Top left: comparison between -12° (7:40a), -24° (8:30a), -36° (9:15a) and -50° (10:10a) at day 16 Apr., 2014. Top right: the same as previous but for -36° (9:15a) and -50° (10:10a) at day 17 Apr. Top right: Bottom left: idem but for -24° (8:30a), -36° (9:15a) at day 18 Apr. Bottom right: ibidem but 0° (6:50a), -12° (7:40a), -24° (8:30a), -36° (9:15a) and -50° (10:10a) at day 19 Apr.

5.2 VEx/VIRTIS-M results

Before comparing results from CFHT/ESPaDOnS and Vex/VIRTIS-M, in this section we compare different results from the VIRTIS-M cloud-tracking technique. As many as 104 wind measurements were obtained with cloud-tracking on the VIRTIS-M images. When confronted with mean profiles of the winds from VEx/VIRTIS-M (Hueso et al., 2015), the zonal and meridional wind speeds display, as expected (Peralta et al., 2007), a clear decrease of the zonal component poleward of mid-latitudes and a weak meridional circulation towards the polar region (see figure 5.8). Also observe that the winds obtained during VEx orbit 2923 display more disperse values in both components, suggestive of winds being affected by the presence of stronger wave activity (see figure 4.3d).

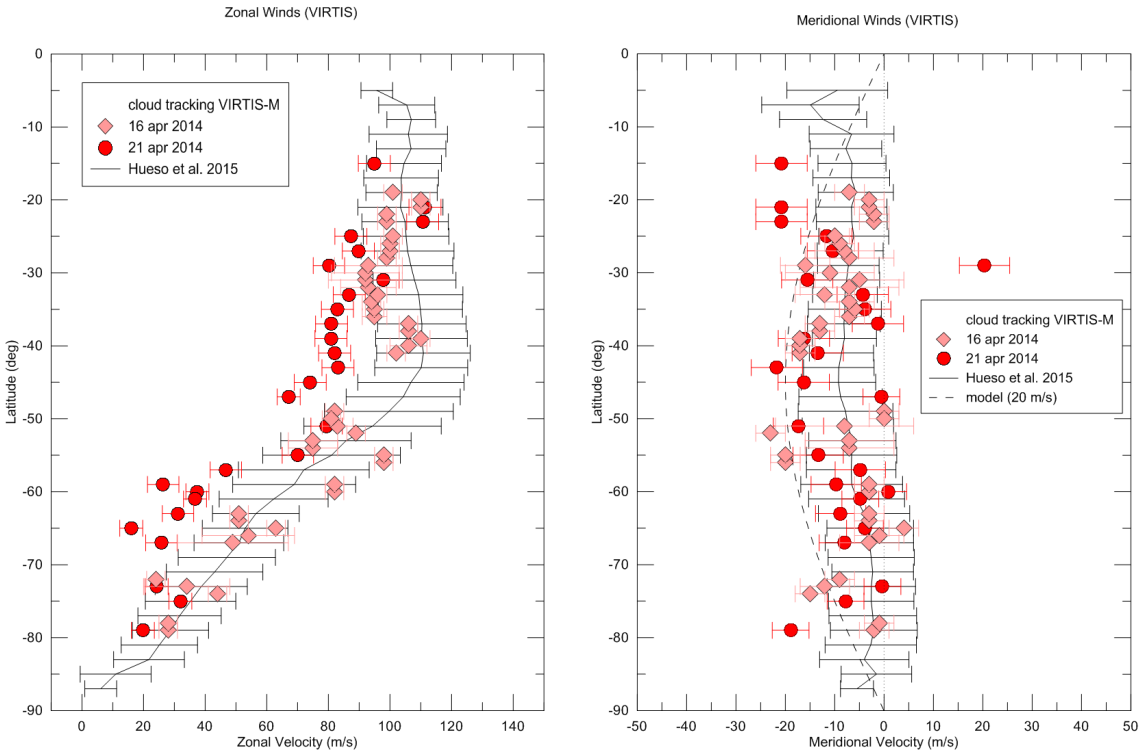

Figure 5.8: Zonal and meridional wind speeds measured with cloud-tracking using VIRTIS-M images taken at 380 nm during the VEx orbits 2918 (diamonds) and 2923 (circles), corresponding to dates 16 and 21 of April 2014. Zonally averaged winds from VIRTIS-M long-term studies are also displayed as reference with black solid line (Hueso et al., 2015). In the case of the meridional winds, the dashed line is a fit to a pure meridional model flow with $\overline{v}_m = (22.5 \pm 15.5)$ m s^{-1} (see table 5.1) as in figure **??**.

5.3 Intercomparison of results (CFHT/VEx)

In this section we compare results from the latitudinal profile for each day of observations with CFHT/ESPaDOnS and VEx/VIRTIS-M (figure 5.9) Each presented latitudinal wind velocity results from a weighed average along each latitude band measured on each day of observations. The weighing coefficients were the inverse of the variance associated to each velocity measurement.

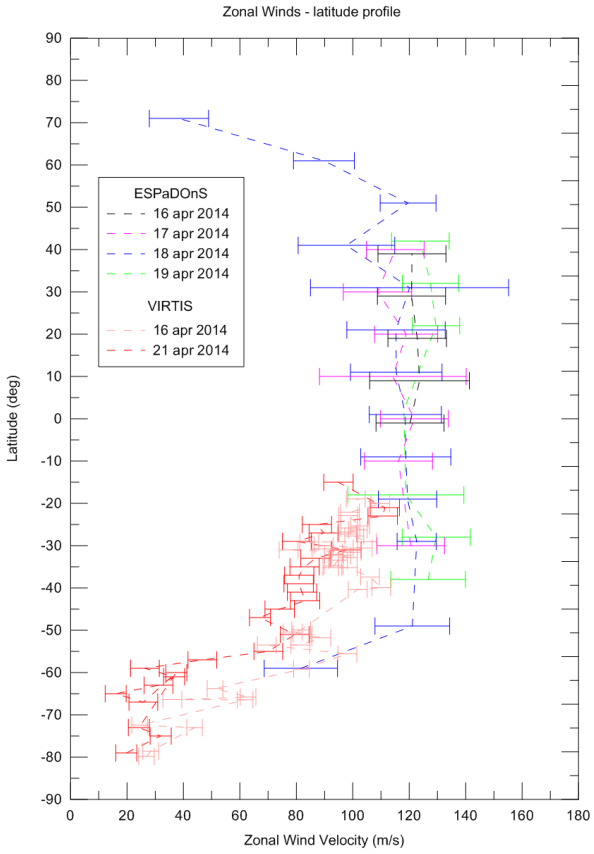

Figure 5.9: Zonal wind velocities $\overline{v}_{z,i}$. Latitudinal profile for each day of observations with CFHT/ESPaDOnS (days 16, 17, 18, 19 April, 2014), and space-based observations with VEx/VIRTIS-M on 16 and 21 April, 2014.

5.3.1 Long-term comparison

In figure 5.10 we compare results from CFHT/ESPaDOnS and Vex/VIRTIS-M from 2014 (this work) and from 2011 (previous work from (Machado et al.,

2014). It is noteworthy the consistency of Doppler velocimetry results from different data (3 years apart), both in zonal and meridional winds. Regarding the VIRTIS-M results, there is a higher dispersion both in zonal and meridional winds. There is also noticeable lower zonal wind velocities relatively to the velocities retrieved by the Doppler velocimetry technique.

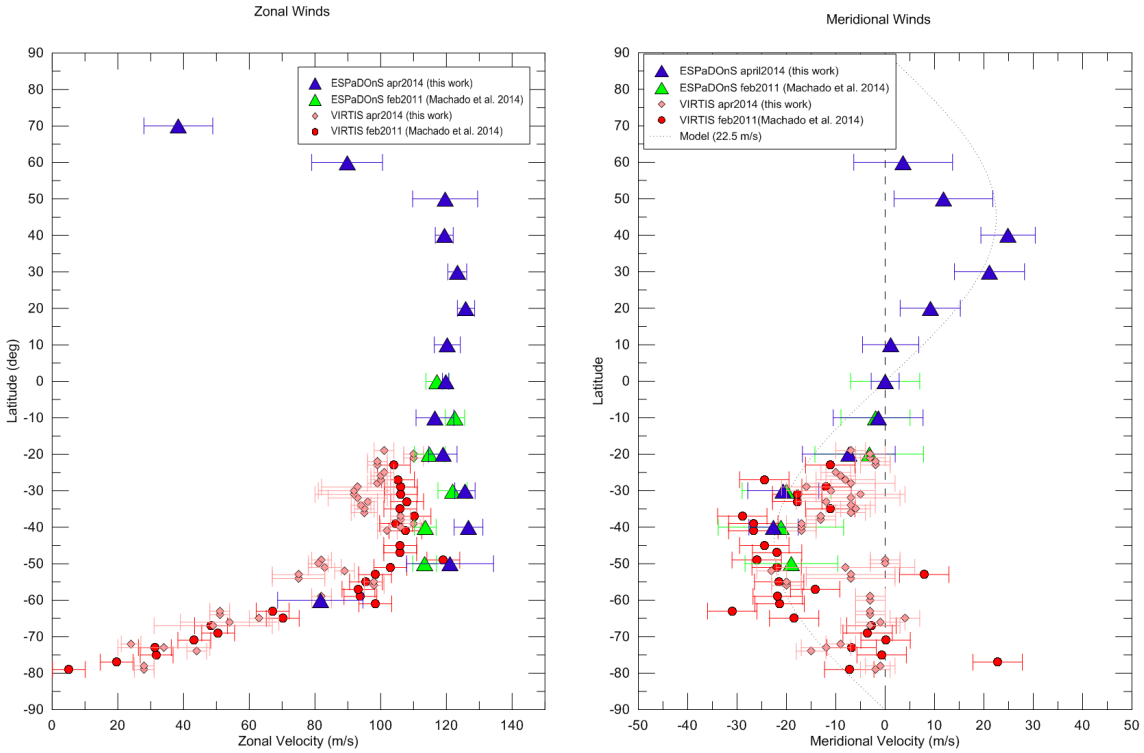

Figure 5.10: Comparison from coordinated CFHT/ESPaDOnS and VEx/VIRTIS-M simultaneous observations. We can compare two distinct runs: April 2014 CFHT/ESPaDOnS' run (blue triangles) and VEx/VIRTIS-M (pink diamonds) show this work latitudinal profile of zonal (left) and meridional (right). We can also compare with the coordinated results from Machado et al. (2014), where green triangles show zonal wind latitudinal profile retrieved from CFHT/ESPaDOnS' observations from February 2011, and red circles come from VEx/VIRTIS-M coordinated observations.

Figure 5.11 presents a comparison of zonal winds obtained at different dates with different techniques:

1. Doppler velocimetry data - (i) CFHT/ESPaDOnS from 2014 (this work) and 2011 (Machado et al., 2014) (ii) VLT/UVES from 2011 (Machado et al., 2012).

2. Cloud Tracking data - Vex/VIRTIS-M from 2014 (this work) and 2011 (Machado et al., 2014).

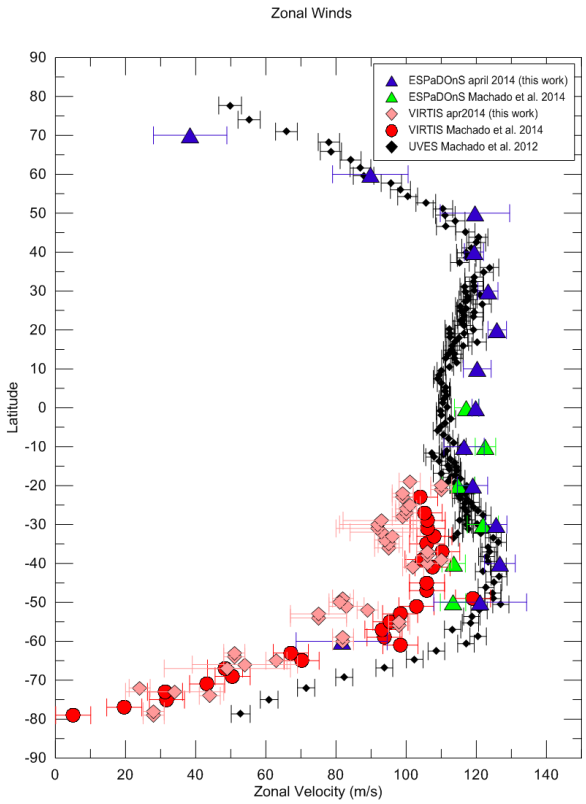

Figure 5.11: Comparison between our Doppler wind measurements and our coordinated cloud-tracked winds. Black diamonds are from VLT/UVES observations (long-slit high-resolution spectroscopy) (Machado et al., 2012). Green triangles from CFHT/ESPaDOnS fiber-fed spectrograph and red circles from coordinated Venus Express VIRTIS-M's observations made on February 2011 (Machado et al., 2014). Finally, blue triangles and pink diamonds (this work) come, respectively, from coordinated observations of the same instruments as the previous cases, these observations were made on April 2014.

The latitudinal wind profile obtained with CFHT/ESPaDOnS are consistent with the complete profile previously obtained in 2007 with UVES at mid-latitudes (figure 5.11). These jet-like structures are moderate, with the southern jet in excess of ∼10 m/s of its northern counterpart.

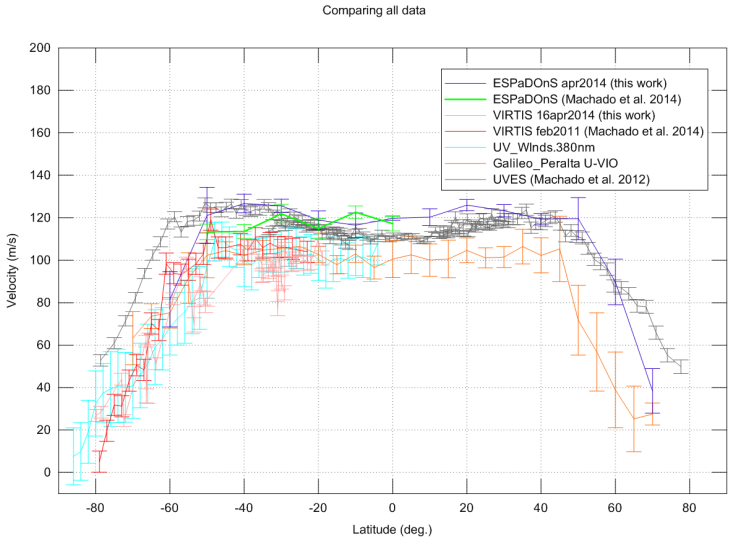

Figure 5.12: Comparison between latitudinal wind profiles obtained using a selection of ground-based and orbiter observations. This paper's results are VIRTIS-M cloud tracking measurements (orange) and CFHT/ESPaDOnS vz;i Doppler winds (purple). VLT/UVES (Machado et al., 2012) absolute zonal wind velocities are shown on grey colour. Winds retrieved at 380 nm in the ultraviolet are shown in light blue come from Sánchez-Lavega et al. (2008). The reanalysis of Galileo results (Peralta et al., 2007) is marked in brown colour.

Chapter 6

Discussion and Conclusions

6.1 Discussion

- Zonal wind latitudinal profile of CFHT/ESPaDOnS $\overline{v}_{z,i}$ velocities obtained from a weighed average on all data present on our observations (table 5.2), and consolidated by the observations from all days of observations, are shown in figure **??**. The weighing coefficients are the inverse of the variance related to each retrieved velocity.

- We note an almost uniform average zonal wind component ($\overline{v}_{z,i}$) between mid-latitudes, the presence of mid-latitudes jets and a steady decrease of zonal wind for higher latitudes (latitudes higher than 50°). Our weighted average is in agreement with wind measurements from cloud tracking using images taken with the VIRTIS instrument (Sánchez-Lavega et al., 2008).

- The zonal winds retrieved from Doppler velocimetry tehcnique (both from CFHT/ESPaDOnS and VLT/UVES) are generally in good agreement with the zonal winds retrived by space-based could-tracking (as seen in figures 5.9, 5.11 and 5.12). However, besides the good agreement between the results from the two techniques, the cloud tracked winds measure slightly lower winds. This is possibly due to altitude level surveyed is variable (cloud tops at different heights), and cloud tracked winds coming essentially from high southern latitudes where cloud deck is compressed (Ignatiev, 2009).

- The meridional wind results presented in figure 5.10 (right) show that both methods (CT and Doppler velocimetry) are consistent and complementary, although the Doppler velocimetry results suffer less dispersion and benefict from lower error bars. This is due to the higher

inertial velocity stability provided by ground-based observations, which is a major technique rquirement.

- On the longitudinal wind variability, the systematic higher wind velocities measured in the sub-terrestrial meridian ($[\phi - \phi_E] = 0°$) can be interpreted in terms of a thermal solar tide, as stated by Machado et al. (2014) and Sánchez-Lavega et al. (2008) (see figures 5.1, 5.4 and 5.5).

- The presence of wind Jets at latitude $\sim$50°(both hemispheres) are not so evident in these results as they were in previous results, with both VEx/VIRTIS-M and VLT/UVES (see figure 5.12. However, ongoing and future observations should contribute to the detection and study of these Jets.

Cloud tracking considerations

Renewed interest in measuring the winds at clouds top from the ground has emerged in the course of the Venus Express mission as well as the Akatsuki mission. However, winds derived by tracking cloud features do not necessarily trace the true circulation. They may instead represent the phase speed of a condensation wave, as in the case of orographic clouds which remain fixed to mountain tops regardless of the wind velocity, while cloud particles are moving at the horizontal wind velocity. In spite of comprehensive wind fields retrieved using the cloud tracking technique, in order to better constrain mesosphere's dynamics, and despite the high spatial resolution allowed by the Venus Express instruments, the wind vectors produced are time averaged ones, so this technique it is not the best research approach to study wind variability and the presence, and propagation, of planetary waves, such as gravity waves and solar lock tide waves. The main purpose of this work is, therefore, to provide instantaneous direct wind velocity measurements using visible Fraunhofer lines scattered by Venus' cloud tops. Thus, our Doppler velocimetry technique constitutes a complementary way of probing the Venus' atmosphere, and a unique approach from the ground, seen that this method measures directly the aerosol particles motion, and the retrieved wind velocities are instantaneous measurements.

6.2 Conclusions

- **Ground and Space: coordinated observations**

  The data taken at CFHT/ESPaDOnS on 16-21 April 2014, in coordination with Vex/VIRTIS measurements, allows monitoring the wind variability at cloud tops. For Doppler velocimetry, at visible wavelengths, the optical depth reaches unity at 70 km (Ignatiev, 2009), which is also the altitude studied with cloud tracking in the UV, with both VEx/VIRTIS and VEx/VMC (Sánchez-Lavega et al., 2008; Moissl et al., 2009). This allows a direct comparison of magnitudes and spatial variations obtained with VLT/UVES, Pioneer Venus, Galileo (SSI) and Venus Express.

- **Doppler velocimetry and Cloud-tracking: complementary techniques**

  The ground-based Doppler velocimetry technique has proven its reliability in constraining global wind circulation models, complementary of space-based measurements. Our Doppler retrievals are in general

good agreement with previous measurements based on cloud tracking (Del Genio and Rossow, 1990; Limaye et al., 2007; Peralta et al., 2007; Sánchez-Lavega et al., 2008; Moissl et al., 2009; Hueso et al., 2015). We retrieved the same order of magnitude and latitudinal variation of Pioneer Venus, Galileo and VEx/VIRTIS measurements, which cross-validates both techniques and provides reasonable confirmation that cloud tracking and Doppler methods both retrieve the velocities of air masses to first order.

- **Comparing wind variability**

  The cloud tracked winds based on VIRTIS-M observations show relevant variability, although it is difficult to compare with the Doppler winds due to a significant interval from the two sets of observations. The variability inherent to atmospheric motions over different time scales, and the temporal and spatial sampling of the data, however, must be taken into account when interpreting velocity measurements.

- **Meridional wind**

  An unambiguous detection of poleward meridional circulation is reported, using optical Doppler velocimetry from the ground at CFHT. We obtained a latitudinal profile of the meridional wind along both North and South hemispheres. The measured meridional wind profile reveals high consistency with a 20 m/s meridional wind model (figure 5.3) and they it is in agreement with a Hadley cell's upper branch, were the meridional wind flows from equator region to higher latitudes. We stress the almost symmetrical behavior of the meridional wind flow between North and South hemispheres. It is noteworthy that if, in the one hand, between mid-latitudes the model is consistent with the measured meridional wind velocities, in the other hand, at high latitudes (after 50°) we can see a systematic discrepancy between measurements and model, which possibly could be related to the presence of the "cold collar". This collar structures are located between 60° and 70° latitude (in both hemispheres), extending trough the polar vortex structure. Thus, this collar structure could be the explanation for such abrupt drop in meridional wind velocity at 60° latitude.

- **Doppler velocimetry technique**

  The Doppler velocimetry is currently the only ground-based technique able to derive instantaneous winds velocities, allowing cross-comparison with cloud tracked winds from VEx VIRTIS-M and VMC UV images, and the study of short term variability.

The meridional wind profile obtained with the groud-based Doppler velocimetry represents a major contribution for our understanding of the dynamics of the Hadley cell. This techniques has shown its consistency and allowed us to retrieve meridional wind profiles with higher precision and decreased error bars relatively to te results obtained with other ground or space observations. These results may be seen as a milestone for future studies and improved modelization of Venus' atmosphere.

Acknowledgements

This research his supported by the European Commission Framework Program FP7 under Grant Agreement 606798 (Project EuroVenus). We thank the VIRTIS/Venus Express team, the European Space Agency, and the Project EuroVenus. I also aknowledge the support of Faculdade de Ciências da Universidade de Lisboa (FCUL), the Fundação da Faculdade de Ciências de Universidade de Lisboa (FFCUL), and the Instituto de Astrofísica e Ciências do Espaço (IA).

Bibliography

Ahrens, D., Meteorology Today, Brooks/Cole-Thomson Learning, 2003.

J. Kelly Beatty, Carolyn Collins Petersen, Andrew Chaikin: *The New Solar System*, 4th Edition, Cambridge University Press, 1999.

Bengtsson, L., and Grinspoon, D., Towards understanding the climate of Venus, (Vol. 11). Springer, 2013.

Blamont, J., Planetary balloons. Exp. Astron. 22, 1-39, 2008.

Bougher, S., Hunten, D. and Philips, R., Upper Atmosphere Dynamics, Global Circulation and Gravity Waves, Venus II: Geology, Geophysics, Atmosphere, and Solar Wind Environment, University of Arizona Press, Tucson, AZ, Bougher S.W, Hunten D.M. and Phillips R.J., Eds., p. 259-291, 1997.

Bullock, A., Grinspoon, D.H., The recent evolution of climate on Venus. Icarus 150, 19-37, 2001.

Cardesín, Study and Implementation of the End-to-End data pipeline for the VIRTIS imaging spectrometer on board Venus Express : From Science operation Planning to Data Archiving and Higher Level Processing", PhD thesis, Centro Interdipartimentale di Studi e Attività Spaziali (CISAS), Universita degli Studi di Padova, 2010.

Chassefière, E., Wieler, R., Marty, B., and Leblanc, F., The evolution of Venus : Present state of knowledge and future exploration, Planetary and Space Science 63-64, 15-23, 2012.

Carlson, R.W., Kamp, L., Baines, K., Pollack, J., Grinspoon, D., Encrenaz, T., Drossart, P., Lellouch, E., and Bezard, B., Variations in Venus cloud particle properties: A new view of Venus's cloud morphology as observed by the Galileo near-infrared mapping spectrometer, Planet Space Sci., 41, 477-486, 1993.

Civeit, T. et al., On measuring planetary winds using high-resolution spectroscopy in visible wavelengths, Astronomy and Astrophysics, volume 431, p. 1157-1166, 2005.

Colin, L., Hunten, D., Pioneer Venus experiment descriptions. Space Sci. Rev. 20, 451-525, 1977.

Del Genio A.D. and Rossow W.B., Planetary-scale waves and the cyclic nature of cloud top dynamics on Venus, Journal of the Atmospheric Sciences, volume 47, p. 293-318, 1990.

Dollfus, A., Venus - evolution of upper atmospheric clouds. J. Atmos. Sci. 32, 1060-1070, 1975b.

Donati, J. F., Semel, M., Carter, B. D., Rees, D. E., Cameron, A. C. Spectropolarimetric observations of active stars. Monthly Notices of the Royal Astronomical Society, 291(4), 658-682, 1997.

Drossart, P., Piccioni, G., Gerard, J.C., et al. A dynamic upper atmosphere of Venus as revealed by VIRTIS on Venus Express. Nature, vol. 450, no 7170, p. 64-645, 2007.

Esposito, L. W., Knollenberg, R., Marov, M., Toon, O. and Turco, R., The clouds and hazes of Venus, in Venus, edited by D.M. Hunten, L. Colin, T.M. Donahue, and V.I. Moroz, pp. 484-564, University of Arizona Press, Tucson, 1983.

Fegley, B., Klingelhofer, G., Lodders, K., Widemann, T., Geochemistry of Surface-Atmosphere Interactions on Venus, Venus II, S.W. Bougher, D.M. Hunten, & R.J. Phillips Eds., University of Arizona Press, Tucson, pp. 591-636, 1997.

Garate-Lopez, I., Hueso, R., Sanchez-Lavega, A., Peralta, J., Piccioni, G., Drossart, P., A chaotic long-lived vortex at the southern pole of Venus, Nature Geoscience 6, 254-25, 2013.

Gierasch, P., Meridional circulation and Venus atmospheric rotation, Journal of the Atmospheric Sciences, volume 32, p. 1038-1044, 1975.

Gierasch, P. et al., The general circulation of the Venus atmosphere: an assessment, Venus II: Geology, Geophysics, Atmosphere, and Solar Wind Environment, University of Arizona Press, Tucson, AZ, Bougher S.W, Hunten D.M. and Phillips R.J., Eds., p. 459-500, 1997.

Goody, R.; Walker, J. Atmosferas Planetárias, Editora Edgard, 1975.

Grinspoon, D.H., Venus Revealed: A New Look Below the Clouds of Our Mysterious Twin Planet (Helix Books, Perseus Publishing, Cambridge, Massachusetts, 1997.

Grinspoon, D.H., Bullock, M., in Astrobiology and Venus Exploration, ed. by L.W. Esposito, E.R. Stofan, T.E. Cravens. Exploring Venus as a Terrestrial Planet (American Geophysical Union, Washington DC, 2007.

Hansen, J.E., Hovenier, J.W., 1974. Interpretation of the polarization of Venus. J. Atmos. Sci. 31, 1137-1160.

Holland, H.D., The Chemistry of the Atmospheres and Oceans, Wiley, New York, 1978.

Hueso R., Peralta J., Garate-Lopez I., Bandos T.V., Sánchez-Lavega, A., Six years of Venus winds at the upper cloud level from UV, visible and near infrared observations from VIRTIS on Venus Express, 2015

Ignatiev, N.I. et al., Altimetry of the Venus cloud tops from the Venus Express observations, Journal of Geophysical Research, vol. 114, E00B43, 2009.

Kasting, J.F., Runaway and moist greenhouse atmospheres and the evolution of Earth and Venus, Icarus, 74, 472-494, 1988.

Kawabata, K., Coffeen, D.L., Hansen, J.E., Lane, W.A., Sato, M., Travis, L.D., Cloud and haze properties from pioneer Venus polarimetry. J. Geophys. Res. 85, 8129-8140, 1980.

Knollenberg, R. G.; Hunten, D. M., The microphysics of the clouds of Venus - Results of the Pioneer Venus particle size spectrometer experiment, Journal of Geophysical Research, vol. 85, p. 8039-8058, 12/1980.

Lellouch, E. et al., Global circulation, thermal structure, and carbon monoxide distribution in Venus' mesosphere in 1991, Icarus, volume 110, no. 2, p. 315-339, 1994.

Lellouch, E. and Witasse, O., A coordinated campaign of Venus ground-based observations and Venus Express measurements, Planetary and Space Science, volume 56, p. 1317-1319, 2008.

Lewis, J. Physics and Chemistry of the Solar System, Elsevier Academic Press, 2004.

Limaye, S.S. et al., Venus Atmospheric Circulation: Known and unknown, volume 112, E04S09, 2007.

Limaye, S.S. et al., Vortex circulation on Venus: Dynamical similarities with terrestrial hurricanes, Geophysical Research Letters, volume 36, L04204, doi:10.1029/2008GL036093, 2009.

Luz, D. et al. Characterization of zonal winds in the stratosphere of Titan with UVES, Icarus, volume 179, p. 497-510, 2005a.

Luz, D. et al. Characterization of zonal winds in the stratosphere of Titan with UVES: 2. Observations coordinated with the Huygens Probe entry, Journal of Geophysical Research, volume 111, CiteID E08S90, 2006.

Luz, D. et al. Venus's Southern Polar Vortex Reveals Precessing Circulation, Science, volume 332, p. 577-580, 2011.

Machado, P., Luz, D. Widemann, T., Lellouch, E., Witasse, O, Characterizing the atmospheric dynamics of Venus from ground-based Doppler velocimetry, Icarus, Volume 221, p. 248-261, 2012.

Machado, P., Widemann, T., Luz, D., Peralta, J., Wind circulation regimes at Venus' cloud tops : Ground-based Doppler velocimetry using CFHT/ESPaDOnS and comparison with simultaneous cloud tracking measurements using VEx/VIRTIS in February 2011, Icarus, 2013.

Machado, P., Widemann, T., Luz, D., Peralta, J., Wind circulation regimes at Venus' cloud tops: Ground-based Doppler velocimetry using CFHT/ESPaDOnS and comparison with simultaneous cloud tracking measurements using VEx/VIRTIS in February 2011, Icarus, 2014.

Markiewicz, W. et al., Morphology and dynamics of the upper cloud layer of Venus, *Nature*, volume 450, p. 633-636, 2007.

Moissl, R. et al., Venus cloud top winds from tracking UV features in Venus Monitoring Camera, Jornal of Geophysical Research, volume 114, E00B31, 2009.

Mueller, N.T., Helbert, J., Erard, S., Piccioni, G., and Drossart, P., Rotation period of Venus estimated from Venus Express VIRTIS images and Magellan altimetry, Icarus, volume 217, p. 474-483, 2011.

Peralta, J., Hueso, R., Sánchez-Lavega, A., A reanalysis of Venus winds at two cloud levels from Galileo SSI images, *Icarus*, volume 190, p. 469-477, 2007.

Peralta, J., Imamura T., Read P., Luz D., Piccialli A., López-Valverde M. A., Analytical Solution for Waves in Planets with Atmospheric Superrotation. I. Acoustic and Inertia-Gravity Waves. Astrophys. J. Suppl. Ser. 213(1), 2014

Peralta, J.; Hueso, R.; Sï¿½nchez-Lavega, A., Characterization of mesoscale gravity waves in the upper and lore clouds of Venus from VEx-VIRTIS images, Journal of Geophysical Research, volume 113, E00B18, 2008.

Piccioni G. et al., South-polar features on Venus similar to those near the north pole, *Nature*, volume 450, p. 637-640, 2007.

Pollack, J., Toon, O. and Boese, R., Greenhouse models of Venus' high surface temperature, as constrained by Pioneer Venus measurements, J. Geophys. Res., 85, 8223-8231, 1980.

Rossow, W., Williams, G., Large-scale motion in the Venus stratosphere, Journal of the Atmospheric Sciences, volume 36, p. 377-389, 1979.

Sánchez-Lavega, A., Hueso, R., Piccioni, G., Drossart, P., Peralta. J., Pï¿½rez-Hoyos, J., Wilson, C., Taylor, F., Baines, K., Luz, D., Erard, S., Lebonnois, S.: Variable winds on Venus mapped in three dimensions, *Geophysical Research Letters*, vol. 35, 2008.

Saunders, R.S., A.J. Spear, P.C. Allin, R.S. Austin, A.L. Berman, R.C. Chandler, J. Clark, A.V. Decharon, E.M. DeJong, D.G. Griffith, J.M. Gunn, S. Hensley, W.T.K. Johnson, C.E. Kirby, K.S. Leung, D.T. Lyons, G.A. Michaels, J. Miller, R.B. Morris, R.G. Pierson, J.F. Scott, S.J. Schaffer, J.P. Slonski, E.R. Stofan, R.W. Thompson, and S.D. Wall, Magellan mission summary, J. Geophys. Res., 97, 13067-13090, 1992.

Suomi, V.; Limaye, S., Venus - Further evidence of vortex circulation, Science, volume 201, p. 1009-1011, 1978.

Taylor, F., McCleese, D., Elson, L., Martonchik, J., Diner, D., Houghton, J., Delderfield, J., Schofield, J., Bradley, S., Infrared remote sensing of the atmosphere of Venus from the Pioneer 12 Orbiter, Space research. Volume 20 - Proceedings of the Open Meetings of the Working Groups on Physical Sciences, Bangalore, India, May 29-June 9, 1979. Oxford and Elmsford, N.Y., Pergamon Press, p. 227-230, 1980.

Taylor, F., Hunten, D. and Ksanfomaliti, L., The thermal balance of the middle and upper atmosphere of Venus, pages 650-680. 1983.

Taylor, F., Grinspoon, D., Climate evolution of Venus, Journal of Geophysical Research, Volume 114, 2009.

Widemann, T. et al., New wind measurements in Venus lower mesosphere from visible spectroscopy, Planetary and Space Science, volume 55, p. 1741-1756, 2007.

Widemann et al., Venus Doppler winds at cloud tops observed with ESPaDOnS at CFHT, Planetary and Space Science, Volume 56, p. 1320-1334, 2008.

Young A., Is the Four-Day "Rotation" of Venus Illusory?, Icarus, volume 24, p. 1-10, 1975.

Young, A.; Schorn, R.; Young, L.; Crisp, D., Spectroscopic observations of winds on Venus, I-technique and data reduction. Icarus, volume 38, p. 435-450, 1979.